Inorganic Chemistry

Article

pubs.acs.org/IC

Spectroscopic and Catalytic Characterization of a Functional $Fe^{III}Fe^{II}$ Biomimetic for the Active Site of Uteroferrin and Protein Cleavage

Sarah J. Smith,[†] Rosely A. Peralta,[‡] Rafael Jovito,[‡] Adolfo Horn, Jr.,[‡] Adailton J. Bortoluzzi,[‡] Christopher J. Noble,[§] Graeme R. Hanson,[§] Robert Stranger,[⊥] Vidura Jayaratne,[⊥] Germán Cavigliasso,[⊥] Lawrence R. Gahan,[†] Gerhard Schenk,[†,¶] Otaciro R. Nascimento,[∥] Angélica Cavalett,[▽] Tiago Bortolotto,[▽] Guilherme Razzera,[▽] Hernán Terenzi,[▽] Ademir Neves,*[,‡] and Mark J. Riley*[,†]

[†]School of Chemistry and Molecular Biosciences and [§]Centre for Advanced Imaging, The University of Queensland, Brisbane 4072, Australia

[‡]Departamento de Química and [▽]Centro de Biologia Molecular Estrutural, Universidade Federal de Santa Catarina, Florianópolis, Santa Catarina 88040-900, Brazil

[⊥]Research School of Chemistry, Australian National University, Canberra 0200, Australia

[¶]Department of Chemistry, National University of Ireland—Maynooth, Maynooth County, Kildare, Ireland

[∥]Instituto de Física, Universidade de São Paulo, 13560-970 São Carlos, São Paulo, Brazil

Supporting Information

ABSTRACT: A mixed-valence complex, $[Fe^{III}Fe^{II}\mathbf{L1}(\mu\text{-}OAc)_2]BF_4{\cdot}H_2O$, where the ligand $H_2\mathbf{L1}$ = 2-{[[3-[((bis(pyridin-2-ylmethyl)amino)methyl)-2-hydroxy-5-methylbenzyl](pyridin-2-ylmethyl)amino]methyl]phenol}, has been studied with a range of techniques, and, where possible, its properties have been compared to those of the corresponding enzyme system purple acid phosphatase. The $Fe^{III}Fe^{II}$ and Fe^{III}_2 oxidized species were studied spectroelectrochemically. The temperature-dependent population of the $S = {}^3/_2$ spin states of the heterovalent system, observed using magnetic circular dichroism, confirmed that the dinuclear center is weakly antiferromagnetically coupled ($H = -2JS_1{\cdot}S_2$, where $J = -5.6$ cm^{-1}) in a frozen solution. The ligand-to-metal charge-transfer transitions are correlated with density functional theory calculations. The $Fe^{III}Fe^{II}$ complex is electron paramagnetic resonance (EPR)-silent, except at very low temperatures (<2 K), because of the broadening caused by the exchange coupling and zero-field-splitting parameters being of comparable magnitude and rapid spin−lattice relaxation. However, a phosphate-bound Fe^{III}_2 complex showed an EPR spectrum due to population of the $S_{tot} = 3$ state ($J = -3.5$ cm^{-1}). The phosphatase activity of the $Fe^{III}Fe^{II}$ complex in hydrolysis of bis(2,4-dinitrophenyl)phosphate ($k_{cat.} = 1.88 \times 10^{-3}$ s^{-1}; $K_m = 4.63 \times 10^{-3}$ mol L^{-1}) is similar to that of other bimetallic heterovalent complexes with the same ligand. Analysis of the kinetic data supports a mechanism where the initiating nucleophile in the phosphatase reaction is a hydroxide, terminally bound to Fe^{III}. It is interesting to note that aqueous solutions of $[Fe^{III}Fe^{II}\mathbf{L1}(\mu\text{-}OAc)_2]^+$ are also capable of protein cleavage, at mild temperature and pH conditions, thus further expanding the scope of this complex's catalytic promiscuity.

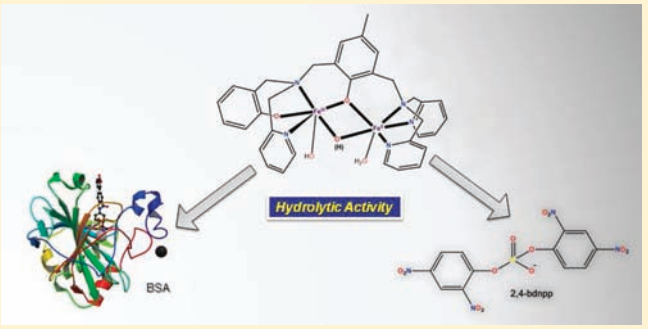

INTRODUCTION

Purple acid phosphatases (PAPs) belong to the family of binuclear metallohydrolases and catalyze hydrolysis of a variety of phosphoester substrates within the pH range of 3−8.[1,2] They are the only binuclear metallohydrolases for which the necessity for a heterovalent active site ($Fe^{III}M^{II}$, where M = Fe, Zn, or Mn) for catalysis has been clearly established. The native pig PAP (uteroferrin) has a Fe_2 active site, and here we report on the spectroscopic and structural characterization of an $Fe^{III}Fe^{II}$ model complex $[Fe^{III}Fe^{II}\mathbf{L1}(\mu\text{-}OAc)_2]^+$, which exhibits a coordination geometry that closely mimics that of uteroferrin. The structural characteristics of the N_2O_2 and N_3O donor atoms provided by the ligand $H_2\mathbf{L1}$ (2-{[[3-[((bis(pyridin-2-ylmethyl)amino)methyl)-2-hydroxy-5-methylbenzyl](pyridin-2-ylmethyl)amino]methyl]phenol}), coupled with the μ-phenoxobis(μ-carboxylato) bridging structure, closely resemble those displayed by the metalloenzyme. Although the complex had been prepared previously,[3,4] its physicochemical properties, especially in relation to the function of the enzyme system, have not been investigated in detail.

Received: August 6, 2011
Published: January 30, 2012

   dx.doi.org/10.1021/ic201711p | *Inorg. Chem.* 2012, 51, 2065−2078

In previous studies,[3,4] it has, however, been established that the $[Fe^{III}Fe^{II}\mathbf{L1}(\mu\text{-OAc})_2]^+$ complex is a good model for the electrochemical properties of uteroferrin, with a redox potential for the $Fe^{III}Fe^{III}/Fe^{III}Fe^{II}$ couple of 380 mV (vs NHE), which compares well with the 344 mV measured for uteroferrin at pH 4.1 via direct electrochemistry[5] and 367 mV at pH 5 via microcoulometry.[6] Magnetic susceptibility data indicate that both Fe centers are high-spin and their bis(μ-acetato)[3] and μ-diphenylphosphato[7] complexes are both weakly antiferromagnetically coupled ($J = -7.4$ and -4.5 cm^{-1}, respectively; $H = -2JS_1 \cdot S_2$). The magnitude of the coupling is similar to that observed for other mixed-valence $Fe^{III}Fe^{II}$ complexes with a bridging phenolate ligand.[8−11]

Mössbauer spectroscopy indicates that the centers are valence-localized at low temperature (with isomer shift and quadrupolar splitting values typical of high-spin Fe^{III} and Fe^{II}), but that some degree of valence detrapping, rapid on the Mössbauer time scale, occurs at room temperature,[3] consistent with the observation of an intervalence charge transfer (CT) in the near-IR (NIR) region.[3]

In this work, we report detailed spectroscopic and computational studies, coupled with an investigation of the hydrolase activity of the complex. These techniques have been employed in order to understand the spectral signatures of the binuclear center and to relate these to the Fe_2 enzyme uteroferrin. A reaction mechanism for the model complex is proposed and compared to that of the corresponding enzyme system. Finally, it is demonstrated that the mixed-valence $Fe^{III}Fe^{II}$ complex is also able to interact and promote the cleavage of bovine serum albumin (BSA) at 37 °C at micromolar concentrations.

MATERIALS AND METHODS

Materials and General Procedures. All reagents were of analytical grade and were purchased from Sigma-Aldrich unless otherwise stated.

Synthesis of $[Fe^{III}Fe^{II}L1(\mu\text{-OAc})_2]BF_4 \cdot H_2O$. $H_2\mathbf{L1}$ was prepared as described previously.[3,4] A mixture of $H_2\mathbf{L1}$ (190 mg, 0.35 mmol), iron(II) tetrafluoroborate tetrahydrate (240 mg, 0.7 mmol), and sodium acetate (120 mg, 1.46 mmol) in methanol (15 mL) was stirred at 40 °C for 30 min, then filtered, and allowed to stand at room temperature. Diffraction-quality, deep-purple crystals were obtained after the solution was allowed to slowly evaporate overnight (145 mg, 47%). Elem anal. Calcd for $C_{38}H_{41}N_5O_7BF_4Fe_2$: C, 51.97; H, 4.71; N, 7.97. Found: C, 52.04; H, 4.59; N, 7.70. Identical material was identified by microanalysis when the same method as that above was followed but ferrous tetrafluoroborate was replaced by equimolar quantities of sodium tetrafluoroborate and ferric chloride. The compound is stable in air in the solid state over a period of months, during which the measurements were completed.

Computational Methods. All calculations were performed with the Amsterdam density functional package,[12−14] and the results reported in the manuscript were obtained using the 2010 version. Functionals based on the generalized gradient approximation and hybrid methodology, and basis sets of both the frozen-core and all-electron types, were utilized. Relativistic effects were included by means of the zero-order regular approximation,[15−17] and the conductor-like screening model was used for the treatment of solvation effects,[18] with H_2O as the solvent.

A detailed description of the functionals and basis sets used in this work is included in the Supporting Information. All results given in the manuscript correspond to calculations using the hybrid model labeled PBE0[19−21] and all-electron basis sets of triple-ζ quality plus one polarization function.[12−14] Electronic excitations were calculated by means of time-dependent density functional theory (TD-DFT)[22] involving a statistical average of orbital potentials model.[23]

Electron Paramagnetic Resonance (EPR) Spectroscopy. Continuous-wave X-band EPR spectra were recorded with a Bruker Biospin Elexsys E580 EPR spectrometer fitted with a superhigh Q cavity. Magnetic-field and microwave-frequency calibration were achieved with a Bruker Biopsin ER 036 M Teslameter and a Bruker Biospin microwave-frequency counter, respectively. Temperatures were controlled using a flow-through cryostat (ESR910) in conjunction with an Oxford ITC503 temperature controller. Spectrometer tuning, signal averaging, and subsequent spectral comparisons were performed with Bruker Biopsin's *Xepr* (version 2.3) software. Computer simulation of the EPR spectrum was performed using *Molecular Sophe* (version 2.0.97).[24]

Magnetic Circular Dichroism (MCD) Spectroscopy. MCD spectra were obtained from samples in an ethanol/methanol (50:50) glass using a 1-mm-path-length quartz cell. The spectra were measured at ±7 T with an Oxford Instruments Spectromag using Hamamatsu R669 PMT and InGaAs detectors, with a Lastek-designed MCD instrument.[25]

Spectroelectrochemical Experiments. Electrochemical experiments (cyclic voltammetry, CV) and spectropotentiostatic experiments were carried out as described elsewhere.[26]

Measurements of Phosphatase-like Activity. Kinetic experiments for hydrolysis of bis(2,4-dinitrophenyl)phosphate (BDNPP) were performed in CH_3CN/H_2O (50:50) media. The pH dependence of the hydrolysis reaction was performed in the pH range 4.50−8.50 at 25 °C. Reactions were carried out using the following conditions: to a 1-cm-path-length cell was added 2000 μL of an aqueous solution ($[buffer]_{final} = 0.05$ mol L^{-1}) of buffers 2-(*N*-morpholino)-ethanesulfonic acid (MES; pH 4.50−6.50) and 4-(2-hydroxyethyl)-1-piperazineethanesulfonic acid (HEPES; pH 7.00−8.50), with $I = 0.05$ mol L^{-1} ($LiClO_4$) and 1250 μL of acetonitrile. This mixture was purged with argon for 20 min. A total of 250 μL of an acetonitrile solution of complex $[Fe^{III}Fe^{II}\mathbf{L1}(\mu\text{-OAc})_2]^+_{final} = 1.30 \times 10^{-5}$ mol L^{-1} was added with a Hamilton syringe, also under an argon atmosphere. The reaction was initiated with the addition of 500 μL of an acetonitrile solution of substrate $[BDNPP]_{final} = 2.50 \times 10^{-3}$ mol L^{-1}, and the reaction was monitored for 15 min.

Corrections for the spontaneous hydrolysis of BDNPP[27] were accomplished by direct difference using a reference cell under identical experimental conditions, without the addition of the catalyst. The initial rates were calculated using molar absorption coefficients (ε) for the release of 2,4-dinitrophenolate at 400 nm given in the literature.[28,29]

The substrate dependence ($[BDNPP]_{final} = 1.5 \times 10^{-3}$–$6.0 \times 10^{-3}$ mol L^{-1}) of the catalytic rate was measured at the optimum pH. Isotopic (deuterium) effects on hydrolysis of BDNP catalyzed by an aqueous solution of $[Fe^{III}Fe^{II}\mathbf{L1}(\mu\text{-OAc})_2]^+$ were investigated by monitoring parallel reactions, where buffer solutions (MES, pH 6.05 and pD 5.89) were prepared in H_2O and D_2O, respectively. The reactions were monitored under a 125-fold excess of substrate at 400 nm. All kinetic data were obtained under an argon atmosphere to prevent oxidation of the $Fe^{III}Fe^{II}$ center to $Fe^{III}Fe^{III}$.

Protein Hydrolysis. Protein cleavage assays were performed using bovine serum albumin (BSA; 66,432.96 Da) as the substrate, as previously described.[30] In a final volume of 20 μL, 30 μmol L^{-1} BSA was treated with a 500 μmol L^{-1} solution of $[Fe^{III}Fe^{II}\mathbf{L1}(\mu\text{-OAc})_2]^+$ for 0−25 h at 37 °C in MES buffer (10 mmol L^{-1}, pH 6.0). Thereafter, each reaction was quenched by chilling the tubes and adding 8 μL of a sample buffer solution (100 mmol L^{-1} Tris-HCl, pH 7.5, 7% SDS, 40% glycerol, 2% β-mercapthoethanol, and 0.01% bromophenol blue). The samples were then subjected to 10% SDS-PAGE. The resulting gels were visualized and digitized using a Kodak Gel Logic 200 (Carestream Health, USA) image system. The BSA that was treated with the solution of $[Fe^{III}Fe^{II}\mathbf{L1}(\mu\text{-OAc})_2]^+$ was also submitted to matrix-assisted laser desorption ionization time-of-flight (MALDI-TOF) mass spectrometry (MS) on an Autoflex III SmartBeam (Bruker, Germany) system to detect possible modifications. After reaction with the solution of $[Fe^{III}Fe^{II}\mathbf{L1}(\mu\text{-OAc})_2]^+$, the protein was precipitated with cold acetone and resuspended in a 20 mmol L^{-1}

dx.doi.org/10.1021/ic201711p | *Inorg. Chem.* 2012, 51, 2065−2078

ammonium bicarbonate buffer. For all analyses, α-cyano-4-hydroxycinnamic acid was used as a MALDI matrix.

Circular dichroism (CD) studies were carried out on a Jasco J-815 spectropolarimeter to determine the changes in the secondary structure of BSA in the presence of $[Fe^{III}Fe^{II}\mathbf{L1}(\mu\text{-}OAc)_2]^+$. A BSA sample (0.5 μmol L^{-1}) in a MES buffer (10 mmol L^{-1}, pH 6.0) at 37 °C was titrated with a solution of $[Fe^{III}Fe^{II}\mathbf{L1}(\mu\text{-}OAc)_2]^+$ to give different ratios of $[Fe^{III}Fe^{II}\mathbf{L1}(\mu\text{-}OAc)_2]^+$/[BSA] ($r$ = 6.6–33). After each addition of the complex, the CD spectra were recorded in a range of 200–300 nm and the spectra were corrected for dilution of the reagents. The spectra of the corresponding buffer and of the complex alone were collected and subtracted from that of the reaction mixture.

RESULTS

X-ray Crystallography. $[Fe^{III}Fe^{II}\mathbf{L1}(\mu\text{-}OAc)_2]BF_4{\cdot}H_2O$ crystallized in the monoclinic space group $P2_1/c$ (crystal data are given as Supporting Information, Table S1), and an ORTEP plot of the cation is given in Figure S1 in the Supporting Information and is schematically shown in Figure 1.

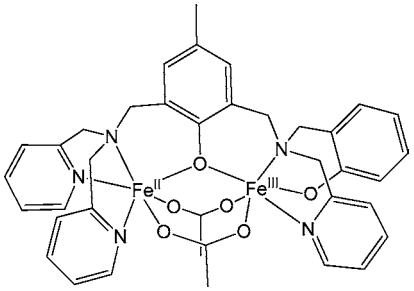

Figure 1. Plot of the $[Fe^{III}Fe^{II}\mathbf{L1}(\mu\text{-}OAc)_2]^+$ cation.

In the cation $[Fe^{III}Fe^{II}\mathbf{L1}(\mu\text{-}OAc)_2]^+$, the bond lengths and bond angles are similar to those previously observed in the perchlorate salt of the complex.[4] The metal–ligand bond lengths are given in Tables S1 and S2 in the Supporting Information, and a bond valence sum (BVS) analysis[28,31] was applied to $[Fe^{III}Fe^{II}\mathbf{L1}(\mu\text{-}OAc)_2]^+$ in order to determine the oxidation states of the Fe centers. The BVS values (3.02 and 2.35) are consistent with the expected high-spin trivalent and divalent oxidation states, respectively (Figure 1).

MS. The electrospray MS spectrum of $[Fe^{III}Fe^{II}\mathbf{L1}(\mu\text{-}OAc)_2]BF_4$ was recorded in both acetonitrile and methanol solvents. In methanol, the major peak corresponds to $[Fe^{III}Fe^{II}\mathbf{L1}(OAc)(OMe)]^+$ (m/z 745), whereas in acetonitrile, the major peak corresponds to the expected intact bis(acetato)-bridged species $[Fe^{III}Fe^{II}\mathbf{L1}(\mu\text{-}OAc)_2]^+$ (m/z 773). In addition, in acetonitrile, peaks corresponding to $[Fe^{III}Fe^{II}\mathbf{L1}(OAc)(OMe)]^+$ (m/z 745; due to the methanolic carrier solvent) and $[Fe^{III}Fe^{II}\mathbf{L1}(OAc)(OOCH)]^+$ (m/z 759) were apparent. Figure 2a shows the MS spectrum in acetonitrile, and the inset shows the expected and observed isotopic distributions of the $[Fe^{III}Fe^{II}\mathbf{L1}(\mu\text{-}OAc)_2]^+$ ion.

The MS spectrum was also recorded in acetonitrile/H_2O (50:50), the same solvent conditions as those employed for kinetic assays (see below). The major peak observed (m/z 688; Figure 2b) can be attributed to $[Fe^{III}_2\mathbf{L1}(OH)(O)]^+$, indicating oxidation of the ferrous ion under the conditions of the electrospray ionization, as has previously been observed in ferrous and other transition-metal-ion complexes.[32–35] Significantly, there is no observation of acetato-bridged species under these conditions. Although MS can yield important information about the structure of species in solution, caution must be

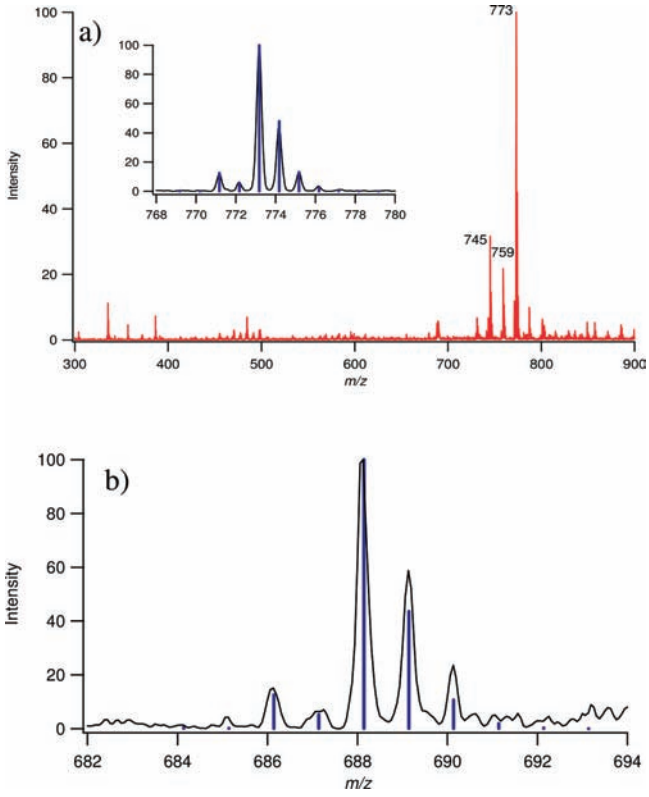

Figure 2. (a) MS spectrum of $[Fe^{III}Fe^{II}\mathbf{L1}(\mu\text{-}OAc)_2]^+$ in acetonitrile. The inset shows the isotopic distributions of the molecular ion (m/z 773) observed and calculated (stick). (b) Dissolution of $[Fe^{III}Fe^{II}\mathbf{L1}(\mu\text{-}OAc)_2]^+$ in acetonitrile/H_2O (50:50). Conditions similar to those used in the kinetic studies produce a major peak (experimental and calculated (stick)) observed at m/z 688 attributable to $[Fe^{III}_2\mathbf{L1}(OH)(O)]^+$.

employed in analysis of the species observed. Experimental artifacts such as redox chemistry under electrospray ionization conditions and the presence of nondetectable neutral species or relatively poor ionizers may influence the species observed.[36]

The MS spectrum of the complex in methanol with an excess of phosphate was also measured (corresponding to EPR conditions vide infra). Under these conditions, the base peak (m/z 848) corresponds to $[Fe^{III}_2(\mathbf{L1}{+}H^+)(PO_4H)_2]^+$, a protonated, doubly phosphato-bridged species. The corresponding sodium (m/z 870) and potassium (m/z 886) adducts were also observed. Peaks corresponding to $[Fe^{III}_2\mathbf{L1}(OAc)(PO_4H)]^+$ (m/z 810) and $[Fe^{III}_2\mathbf{L1}(OMe)(OH_2)_2(PO_4H)]^+$ (m/z 818) were also present.

Spectroelectrochemistry. CV of $[Fe^{III}Fe^{II}\mathbf{L1}(\mu\text{-}OAc)_2]^+$ recorded in CH_3CN displayed two reversible redox processes at +0.38 and −0.49 V (vs NHE), attributed to the successive reductions of $Fe^{III}Fe^{III}$ to $Fe^{III}Fe^{II}$ and $Fe^{III}Fe^{II}$ to $Fe^{II}Fe^{II}$, respectively, with a comproportionation constant of 7.3×10^{14}.[3,37] The magnitude of this constant indicates substantial stability of the $[Fe^{III}Fe^{II}\mathbf{L1}(\mu\text{-}OAc)_2]^+$ complex compared with other mixed-valent $Fe^{III}Fe^{II}$ species described in the literature.[38,39] On the basis of this information, we have used spectroelectrochemistry under the same experimental conditions as those employed in the CV experiments to examine the electronic absorption and redox properties of the oxidized $[Fe^{III}_2\mathbf{L1}(\mu\text{-}OAc)_2]^{2+}$ species (Figure 3) generated in solution from $[Fe^{III}Fe^{II}\mathbf{L1}(\mu\text{-}OAc)_2]^+$.

dx.doi.org/10.1021/ic201711p | Inorg. Chem. 2012, 51, 2065–2078

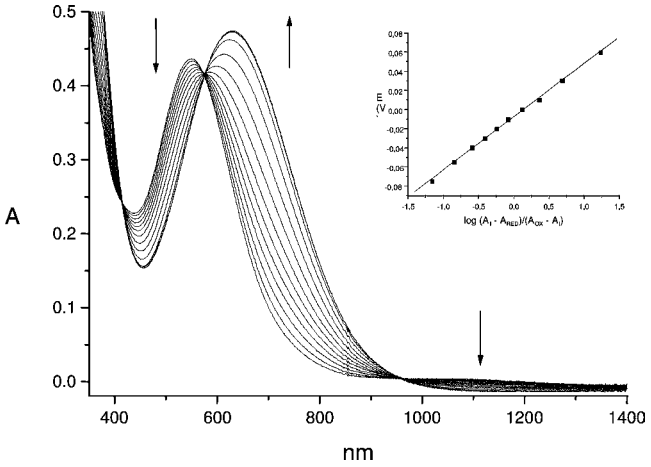

Figure 3. Spectra recorded during a spectropotentiostatic experiment with 1×10^{-5} mol L^{-1} $[Fe^{III}Fe^{II}\mathbf{L1}(\mu\text{-OAc})_2]^+$ (0.1 mol L^{-1} $TBAPF_6$) in CH_3CN. Applied potentials in V vs SCE are as follows: −0.075; −0.055; −0.040; −0.030; −0.020; −0.010; −0.000; 0.010; 0.030; 0.060.[37].

The maintenance of strict isosbestic points in successive spectra strongly suggests the presence of a single product throughout the course of electrolysis, during which the absorption maximum at 551 nm of the mixed-valent species changes to 633 nm with the concomitant disappearance of the broad intervalence CT band centered at ∼1050 nm. $E_{1/2}$ = −0.008 V versus Fc^+/Fc (+0.392 V vs NHE) and n = 1.0 ± 0.1 electrons obtained from the Nernst plot (Figure 3, inset) are in very good agreement with the CV results. It is interesting to note that oxidation of the $Fe^{III}Fe^{II}$ complex (λ_{max} = 551 nm; ε = 4600 L mol^{-1} cm^{-1}) to the corresponding $Fe^{III}Fe^{III}$ species (λ_{max} = 633 nm; ε = 4900 L mol^{-1} cm^{-1}) is accompanied by a small change in the intensity of the absorption band, which suggests that the relevant transitions in both the $Fe^{III}Fe^{II}$ and $Fe^{III}Fe^{III}$ species originate mainly from the terminal phenolate to Fe^{III} CT complex. Similar spectral behavior has been observed in the interconversion of oxidized and reduced PAPs in which the nonreducible Fe^{III} center is coordinated by a terminal tyrosinate residue.[40]

MCD Spectroscopy. The MCD spectrum of $[Fe^{III}Fe^{II}\mathbf{L1}(\mu\text{-OAc})_2]^+$ in an ethanol/methanol glass is shown in Figure 4a, with the dominating positive peak of the ligand-to-metal CT (LMCT) band at 560 nm. Simultaneous fitting of the MCD and absorption spectra required a minimum of four Gaussian bands, at energies of ∼33 300, 24 880, 19 570, and 17 240 cm^{-1}, respectively. In the NIR region, very weak negative and positive features are observed (Figure 4b).

The spectrum is fitted with Gaussian bands at 7600, 11 370, and 12 150 cm^{-1}. The low-energy peak may be due to the intervalence CT transition but is shifted compared to the absorption spectrum, while the latter are likely due to Fe^{II} d−d bands, which are expected to be relatively intense in the MCD spectrum. Variable-temperature (VT) MCD measurements of the complex reveal an unusual temperature-dependent behavior. As shown in Figure 4a, as the temperature is increased, the major bands present at low temperature decrease in intensity, displaying typical *C*-term behavior. However, an additional band at ∼428 nm grows in, presumably arising from population of a low-lying excited state. In order to quantify the area of this band as a function of the temperature, each spectrum was analyzed separately. The band positions

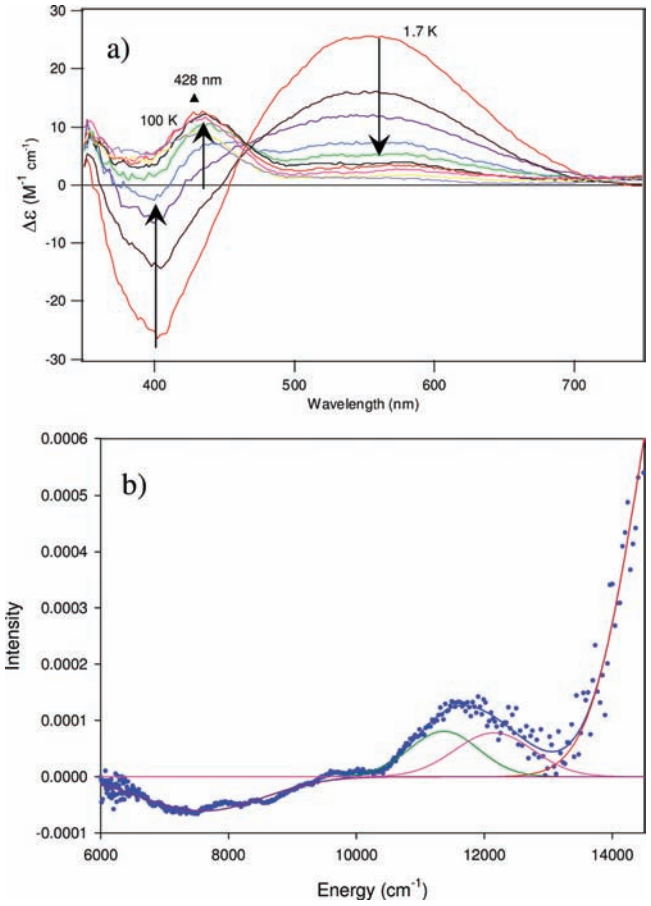

Figure 4. (a) MCD spectrum of $[Fe^{III}Fe^{II}\mathbf{L1}(\mu\text{-OAc})_2]^+$ in a methanol/ethanol glass measured at 5 T at temperatures ranging from 1.7 to 100 K. (b) Gaussian resolved bands in the infrared region of the MCD spectrum.

previously fitted to the lowest-temperature spectrum were fixed for each temperature, and the residual area was fitted to a band centered at 428 nm. The area of this band as a function of the temperature is shown in Figure 5a; below 10 K, the 428 nm band was not detectable. These data can be analyzed using a Boltzmann distribution, fitting the intensity of this band to population of the first $S = {}^3/_2$ excited state as a proportion of the total population.

In the strong exchange ($|J| > |D|$) coupling regime, the antiferromagnetically coupled spins of an Fe^{II} ($S_1 = 2$) and Fe^{III} ($S_2 = {}^5/_2$) binuclear system interact to give five $S_{tot} = {}^1/_2$, ${}^3/_2$, ${}^5/_2$, ${}^7/_2$, ${}^9/_2$ spin states, as shown on the right-hand side of Figure 5a.

From an $H = -2JS_1 \cdot S_2$ exchange coupling Hamiltonian, population of a particular S state as a proportion of the total population is given by[41]

$$P(S) = \frac{(2S+1)e^{JS(S+1)/kT}}{\sum_{S_{tot}}(2S_{tot}+1)e^{JS_{tot}(S_{tot}+1)/kT}} \quad (1)$$

From the fit of eq 1 to the data, an exchange coupling value of J = −5.6 ± 0.5 cm^{-1} is obtained.

VT MCD is an alternate method for analysis of the MCD data and involves collection of the intensity data at a fixed wavelength and a low field, which avoids the possible crossover of sublevels.[42,43] VT MCD data were collected at 580 nm and

dx.doi.org/10.1021/ic201711p | *Inorg. Chem.* 2012, 51, 2065−2078

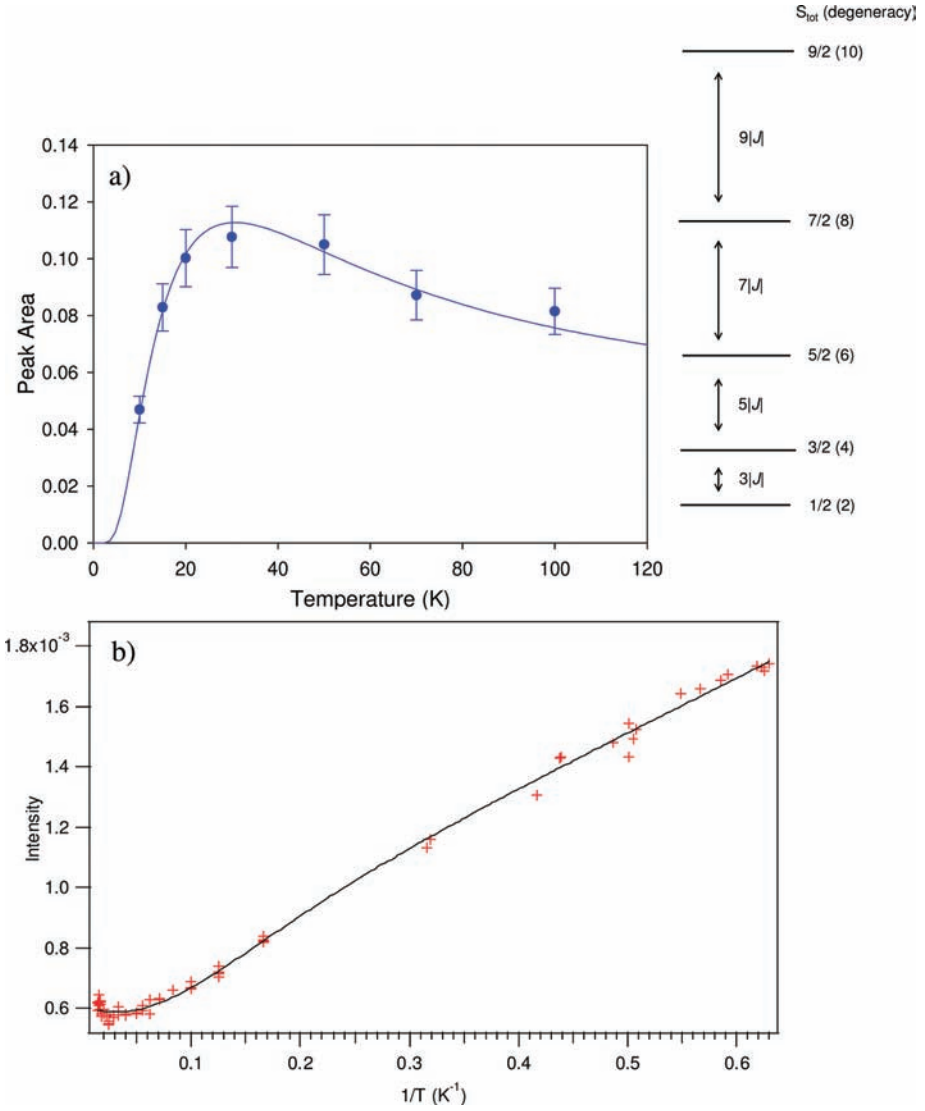

Figure 5. (a) Plot of area of the MCD band at 428 nm as a function of the temperature (left) and energy levels in a coupled $S_1 = {}^5/_2$, $S_2 = 2$ dimer system (right). The solid line shows the best fit to eq 1. (b) Intensity of the MCD at 580 nm and 0.5 T plotted against $1/T$ (K^{-1}). The solid line shows the best fit to eq 2.

0.5 T between 1.6 and 70 K. The intensity versus $1/T$ data is not linear in the high-temperature region (Figure 5b), and again the deviation results from population of a low-lying excited state as the temperature is increased.[42,43] To fit these data, the MCD intensity is expressed as[42]

$$\Delta\varepsilon = \sum_i \left(\frac{C_i}{kT}\alpha_i + B\right)H \qquad (2)$$

where $\Delta\varepsilon$ is the experimental MCD intensity, B accounts for field-induced mixing of the ground and excited states, C_i is the MCD C-term intensity parameter, and α_i is the Boltzmann population of the ith level.[42] The best fit of the intensity at 580 nm versus $1/T$ data to eq 2 is shown in Figure 5b (solid line) with the parameters given in Table 1. The key parameter determined is E_1, the energy of the first excited state, which, given that the energy gap between the two lowest states is $-3J$, corresponds to a J value of -3.4 ± 1 cm^{-1}. While the two values of J are given in Table 1, the second $J = -5.6$ cm^{-1} is preferred because the $J = -3.4$ cm^{-1} value has a higher uncertainty associated with it because of the MCD transitions being weak at low field.

Table 1. MCD Data

B^a	0.000 61
C_0	0.0025
C_1	−0.0063
E_1 (cm^{-1})	10.1
J (cm^{-1})	-3.4 ± 1 to -5.6 ± 0.5^b

[a]Symbols refer to eq 2. [b]This value is from fitting of the 428 nm peak to eq 1.

EPR Spectroscopy. EPR measurements of the complex in the solid state, dissolved in methanol, acetonitrile, or acetonitrile/toluene at temperatures of 2 K or greater yielded a very broad unresolved feature centered around $g \sim 2$, a consequence of rapid spin−lattice relaxation through the Orbach process.[44] At very low temperatures (1 K), the EPR spectrum (Figure S2 in the Supporting Information) of the anaerobically one-electron-reduced binuclear Fe^{III} complex reveals resonances at $g_1 = 1.28$, $g_2 = 1.49$, and $g_3 = 1.74$,

dx.doi.org/10.1021/ic201711p | Inorg. Chem. 2012, 51, 2065−2078

which are typical of an antiferromagnetically coupled high-spin (^{6}A state) Fe^{III} ion with a high-spin (^{5}T state) Fe^{II} ion, resulting in a $S_{tot} = {}^1/_2$ ground state. This is in agreement with magnetic studies that show that the Fe^{II} and Fe^{III} centers in $[Fe^{III}Fe^{II}\mathbf{L1}(\mu\text{-OAc})_2]^+$ are weakly antiferromagnetically coupled in the solid state ($J = -7.4$ cm^{-1})[3] and with the MCD in solution ($J = -5.6$ cm^{-1}; vide supra). Similarly, at pH > 5, bovine spleen PAP exhibits a rhombic spectrum with apparent g values of 1.58, 1.73, and 1.85.[45] The fact that (i) the redox potential for the $Fe^{III}Fe^{III}/Fe^{III}Fe^{II}$ process of $[Fe^{III}Fe^{II}\mathbf{L1}(\mu\text{-OAc})_2]^+$ is similar to that observed for the corresponding couple in uteroferrin and that (ii) the spin-Hamiltonian parameters are at least qualitatively comparable to those obtained for bovine spleen and pig PAPs strongly suggests that the electron density (Lewis acidity) around the Fe^{II} ion is similar in the biomimetic and $Fe^{III}Fe^{II}$ PAPs. The resonances observed at $g_{eff} = 4.3$ and 7.5 in the spectra of $[Fe^{III}Fe^{II}\mathbf{L1}(\mu\text{-OAc})_2]^+$ measured at 1 K (Figure S2 in the Supporting Information) are saturated and arise from a small paramagnetic impurity of the mononuclear Fe^{III} complex.

When phosphate (2 μL, 0.5 mol L^{-1} Na_2HPO_4) was added to a methanolic solution of the complex (500 μL, 1 mmol L^{-1}), the solution changed color from purple to red/orange. The MS spectrum (vide supra) indicates that a phosphate-bridged species ($[Fe^{III}_2(\mathbf{L1}+H^+)(PO_4H)_2]^+$) is formed under these conditions. The EPR spectrum was measured at a number of temperatures between ~2 and 55 K. At the lowest temperature (~2 K), the only resonances ($g_{eff} = 4.3$) observed were those from magnetically isolated high-spin Fe^{III} and a very weak, broad feature at $g \sim 2$. Numerous features emerge upon increasing temperature, as is seen in the spectra measured at 10 and 50 K (Figure 6a,b).

The intensity of the resonances change as a function of the temperature, but their line-shape remains constant. This behavior is typical of an antiferromagnetically coupled (strong exchange regime) binuclear homodivalent high-spin Fe center with an $S_{tot} = 0$ spin ground state, which likely results from oxidation of the $Fe^{III}Fe^{II}$ complex to Fe^{III}_2 in the presence of an excess of phosphate. Fitting the temperature dependence of the resonances (inset in Figure 6) using eq 1 and taking into account the Zeeman splitting and their relative populations indicate that the intense resonances arise from an $S_{tot} = 3$ spin state and that $J = -3.5 \pm 0.5$ cm^{-1}. Because the magnitude and orientation of the zero-field-splitting (ZFS) tensors for the two nonequivalent Fe^{III} centers are unknown, an effective spin Hamiltonian[46] (eq 3) for $S_{tot} = 3$ rather than a complete spin Hamiltonian for the coupled center was chosen to interpret the spectrum.

$$\begin{aligned} H_S &= \beta B\cdot g_S\cdot S_{tot} + S_{tot}\cdot D_S\cdot S_{tot} \\ &\quad + B_4{}^0[35S_{z,tot}{}^4 + 25S_{z,tot}{}^2 - 30S_{z,tot}{}^2S_{tot} \\ &\quad (S_{tot}+1) + 3(S_{tot}(S_{tot}+1))^2 \\ &\quad - 6S_{tot}(S_{tot}+1)] \\ g_S &= c_1g_1 + c_2g_2 \\ D_S &= d_1D_1 + d_2D_2 + d_{12}D_{12} \end{aligned} \tag{3}$$

where $c_1 = c_2 = {}^1/_2$ for a binuclear high-spin Fe^{III} complex and $d_1 = d_2 = -{}^1/_{45}$ and $d_{12} = +{}^{47}/_{90}$ for an $S_{tot} = 3$ spin state.[46] The contributions of D_1 and D_2 to D_S will be minimal because the projection coefficients for this spin state are very small, which, in turn, results in observation of multiple resonances with narrow linewidths because distributions of D_1 and D_2 will also be small.[41,47] In contrast, resonances arising from the other spin states ($S_{tot} = 1$, 2, 4, and 5) will be significantly broader as a consequence of a distribution of D values.[48,49] In binuclear Mn^{II} complexes, which are isoelectronic with binuclear Fe^{III}, it has also been noted that the most resolved spectroscopic features arise from the $S_{tot} = 3$ spin state.[50,51] Computer simulation of the EPR spectrum employing eq 3 ($g_S = 2.0$, $D_S = 717 \times 10^{-4}$ cm^{-1}, $E_S/D_S = 0.0352$, and $B_4{}^0 = 29 \times 10^{-4}$ cm^{-1}) was used to obtain the spectrum shown in Figure 6c, which is in good agreement with the experimental spectrum measured at 50 K (Figure 6b). When a point dipole−dipole approximationis employed, an internuclear distance of 3.36 Å between the Fe^{III} centers can be calculated from the ZFS,[24] in good agreement with the metal−metal distance in oxidized uteroferrin.[2]

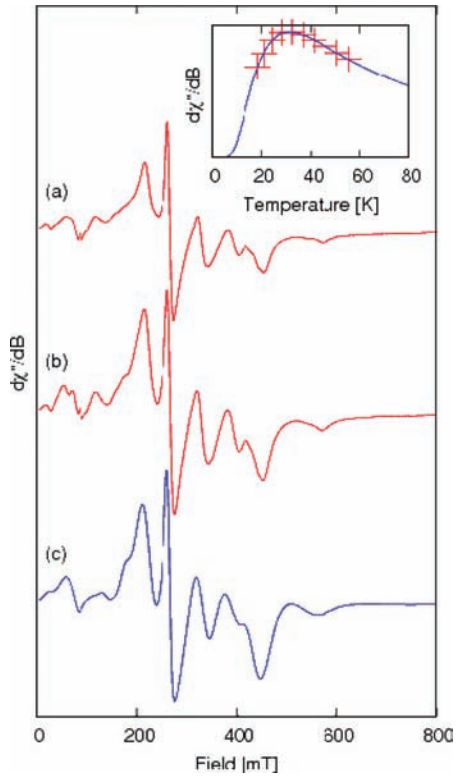

Figure 6. EPR spectra of $[Fe^{III}Fe^{II}\mathbf{L1}(\mu\text{-OAc})_2]BF_4$ dissolved in methanol with an excess of phosphate at (a) 10 K and (b) 50 K (4.00 G modulation amplitude, 2 mW power, and 9.380687 GHz microwave frequency). The inset shows the change in intensity of the resonance at $B = 268.2$ mT as a function of the temperature (points) and the best fit (blue line) to an $S_{tot} = 3$ spin state. See the text for details. (c) Computer simulation of the EPR spectrum shown in part b using the spin-Hamiltonian parameters given in the text.

Electronic Structure Calculations. Table 2 compares the crystallographic and the calculated geometry-optimized structures for the $[Fe^{III}Fe^{II}\mathbf{L1}(\mu\text{-OAc})_2]^+$ complex in columns 2 and 3, respectively.

The average absolute deviation and maximum deviation between calculation and experiment are respectively ~0.02 and ~0.04 Å, which can be considered highly satisfactory for complexes of this size and structural complexity. Mulliken population analysis results (Table S4 in the Supporting Information) are consistent with BVS analysis showing Fe1 = Fe^{III} and Fe2 = Fe^{II} and with the presence of high-spin configurations in all cases, that is, $S = {}^5/_2$ and 2, respectively, for

dx.doi.org/10.1021/ic201711p | Inorg. Chem. 2012, 51, 2065−2078

Table 2. Selected Bond Lengths (Å) of $[Fe^{III}Fe^{II}L1(\mu\text{-}OAc)_2]BF_4{\cdot}H_2O$ and the Calculated Bond Lengths for $[Fe^{III}Fe^{II}L1(\mu\text{-}X)_2]$[a]

	experiment		calculated	
	$Fe^{III}Fe^{II}$		$Fe^{III}Fe^{III}$	
bond	X = $CH_3CO_2^-$	X = $CH_3CO_2^-$	X = $CH_3CO_2^-$	X = HPO_4^{2-}
Fe1−N1	2.21	2.22	2.18	2.22
Fe1−N2	2.18	2.19	2.16	2.20
Fe1−O1	2.01	2.00	2.11	2.18
Fe1−O2	1.88	1.92	1.87	1.91
Fe1−O4	1.95	1.99	2.01	1.93
Fe1−O6	2.03	2.04	2.04	1.97
Fe2−N3	2.20	2.23	2.18	2.23
Fe2−N4	2.22	2.19	2.14	2.20
Fe2−N5	2.18	2.19	2.14	2.16
Fe2−O1	2.10	2.14	1.99	2.01
Fe2−O3	2.13	2.15	2.01	1.95
Fe2−O5	2.04	2.05	1.96	1.90
Fe1···Fe2	3.48	3.49	3.49	3.59

[a]The atomic numbering is given in Figure S1 and Table S2 in the Supporting Information.

Fe^{III} and Fe^{II} sites. The most significant orbital interactions occur between the metal centers and the bridging phenoxo group and between the terminal phenolate group and the Fe^{III} center, as shown in Figure 7.

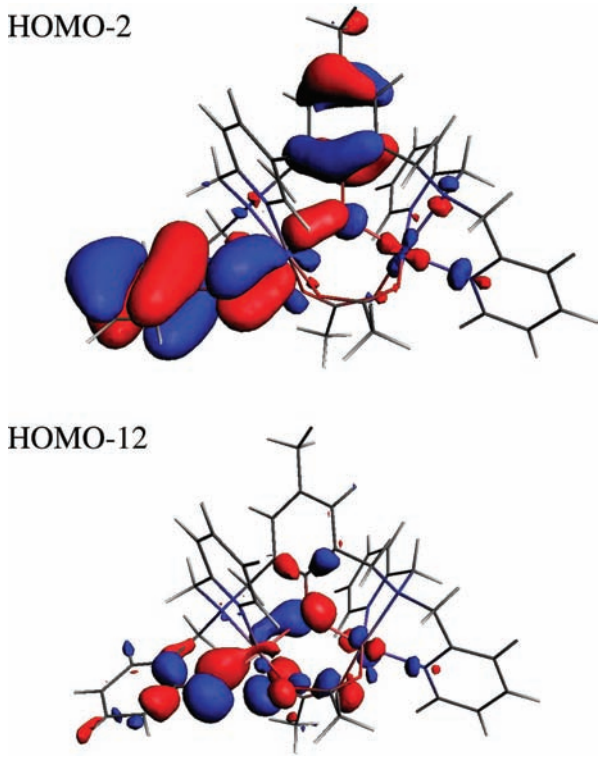

Figure 7. Spatial plots of the HOMO−2 and HOMO−12 levels of $[Fe^{III}Fe^{II}L1(\mu\text{-}OAc)_2]^+$ showing (top) the interaction between the Fe^{III} and Fe^{II} centers via the orbitals on the bridging phenoxo oxygen and (bottom) the interaction between the terminal phenolate and the Fe^{III} center.

The TD-DFT calculations on these systems predict that the low-energy, high-intensity transitions exhibit significant orbital components that involve excitations from (occupied) levels with strong terminal phenolate character to (virtual) levels with strong metal-based character (Figures S5 and S6 in the Supporting Information), in good agreement with spectroscopic (MCD) data reported for uteroferrin.[46]

The good structural agreement for the $[Fe^{III}Fe^{II}L1(\mu\text{-}OAc)_2]^+$ ion allows us to consider the possible species giving rise to the observed EPR signal in the phosphate buffer. The effect of oxidizing Fe^{II} to Fe^{III} at the Fe2 site, given in the last two columns of Table 2, is mainly to reduce the bond lengths of the harder oxygen ligands, while the bond lengths to the N ligands are relatively unchanged. The reduction of the Fe2−O1 bond length of the bridging phenolate results in a concomitant increase in the Fe1−O1 bond distance, which leaves the Fe1···Fe2 distance and Fe1−O1−Fe2 angle relatively unchanged. The replacement of the acetate with HPO_4^{2-} ions results in a decrease of the bond lengths to the phosphate O atoms and an increase in the other bond lengths (Table 2, column 5).

The coordination geometry imposed for the phosphate-bridged systems (in the computational models) is analogous to that found in the crystal structure of the acetate-bridged species, although the predicted Fe1···Fe2 distance (3.59 Å) is slightly longer than that derived from EPR measurements (3.36 Å). The presence of a small anisotropic exchange contribution may be responsible for the slightly smaller internuclear Fe1···Fe2 distance determined by EPR. The isotropic exchange coupling constant was calculated by combining the results for the antiferromagnetic (broken symmetry = BS) and ferromagnetic (high spin = S_{max}) ground-state energy, according to[52,53]

$$E(S_{max}) - E(BS) = -J\left(S_{max} + \frac{1}{2}\right)\left(S_{max} - \frac{1}{2}\right) \quad (4)$$

where $S_{max} = {}^9/_2$. The computationally determined value of $J = -7.9$ cm^{-1} is in both qualitative and quantitative agreement with experimental observations.

Phosphatase-like Activity. Figure 8a illustrates the pH dependence of the phosphatase-like activity of $[Fe^{III}Fe^{II}L1(\mu\text{-}OAc)_2]^+$ in anaerobic acetonitrile/buffer (50:50) solutions, thus preventing oxidation of the complex. The data were fitted to eq 5,[54] which describes two pK_a's (5.03 and 6.93; Table 3) and two catalytically active species.

Note that the activity at high pH does not go to zero and that the activity of the species at higher pH is related to the activity of the species at optimum pH by the constant γ ($V_2 = \gamma V_0$, where V_2 is the limiting rate at high pH), with $V_0 = 3.92 \times 10^{-9}$ mol L^{-1} s^{-1} and $\gamma = 0.3$.

$$V = V_0 \frac{1 + \frac{\gamma K_{a2}}{[H^+]}}{1 + \frac{[H^+]}{K_{a1}} + \frac{K_{a2}}{[H^+]}} \quad (5)$$

The substrate dependence of the complex was measured at pH 5.6, the optimum pH. At this pH, Michaelis−Menten behavior is observed (Figure 8b), yielding $k_{cat.} = (1.88 \pm 0.09) \times 10^{-3}$ s^{-1} and $K_m = 4.63 \pm 0.38$ mmol L^{-1} with 5 turnovers in 20 h. The relatively large errors associated with these values are due, in part, to the poor solubility of the substrate, which precludes measurements at higher substrate concentrations.

dx.doi.org/10.1021/ic201711p | Inorg. Chem. 2012, 51, 2065−2078

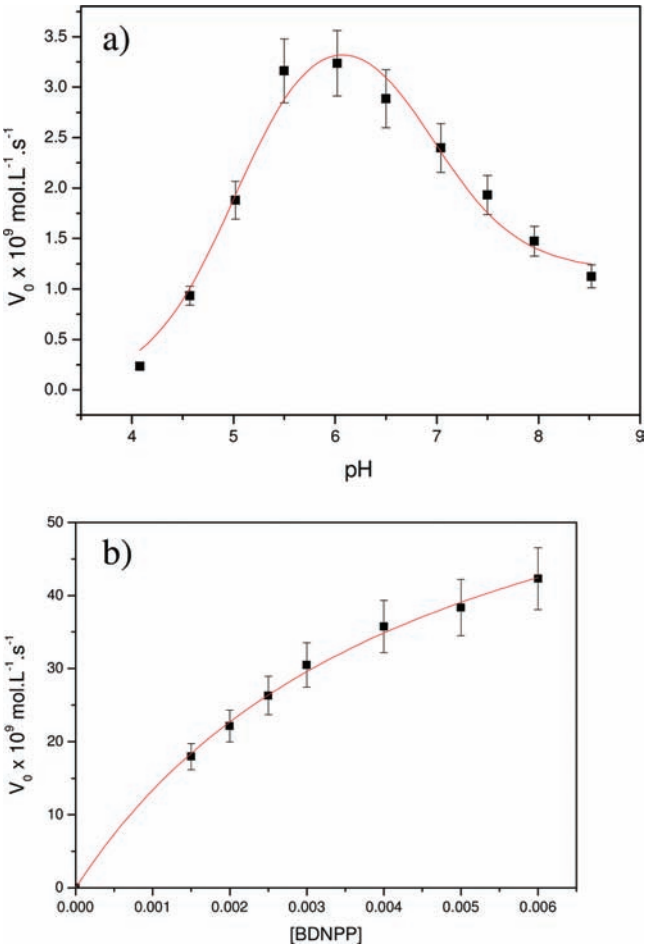

Figure 8. (a) pH dependence of the reaction rate of aqueous solutions of $[Fe^{III}Fe^{II}\mathbf{L1}(\mu\text{-}OAc)_2]^+$, under the following conditions: argon atmosphere, 1:1 H_2O/CH_3CN solution, $[Fe^{III}Fe^{II}\mathbf{L1}(\mu\text{-}OAc)_2]^+ = 1.3 \times 10^{-5}$ mol L^{-1}, [BDNPP] = 2.5×10^{-3} mol L^{-1}, [buffer] = 0.05 mol L^{-1} (buffer = MES, HEPES, and CHES), I = 0.05 mol L^{-1} ($LiClO_4$). (b) Dependence of the reaction rate on the BDNPP concentration for the hydrolysis reaction catalyzed by the aqueous solution of $[Fe^{III}Fe^{II}\mathbf{L1}(\mu\text{-}OAc)_2]^+$ (see Scheme 1) under the following experimental conditions: 1:1 H_2O/CH_3CN at pH 5.6 with a MES = 0.05 mol L^{-1} buffer; I = 0.05 mol L^{-1} ($LiClO_4$); $[Fe^{III}Fe^{II}\mathbf{L1}(\mu\text{-}OAc)_2]^+ = 4.0 \times 10^{-5}$ mol L^{-1}; [BDNPP] = $(1.5\text{–}6.0) \times 10^{-3}$ mol L^{-1}; T = 25 °C.

Table 3. pK_a Values of the Species Described by Scheme 1, As Determined by Potentiometry and Kinetic Analysis[4]

	kinetic	potentiometric
pK_{a1}		3.02
pK_{a2}	5.03	4.13
pK_{a3}		5.76
pK_{a4}	6.93	7.53

We also tested the ability of an aqueous solution of $[Fe^{III}Fe^{II}\mathbf{L1}(\mu\text{-}OAc)_2]^+$ to hydrolyze the monoester (2,4-dinitrophenyl)phosphate (2,4-DNPP) directly with an excess of the substrate; however over a period of 24 h, only the background reaction with the formation of small amounts of 2,4-dinitrophenolate and inorganic phosphate was observed. A similar behavior was observed for the isostructural $Fe^{III}Zn^{II}$[29] and $Fe^{III}Co^{II}$ complexes[55] and is not surprising because second coordination features have been shown to be important for hydrolysis of phosphomonoesters.[56] Finally, the deuterium kinetic isotope effect k_H/k_D = 0.92 obtained under the same conditions as those with H_2O support the idea that no proton transfer is involved in the rate-limiting step of the reaction.

Potentiometric Titrations. Potentiometric titrations were used to determine the pK_a's of the complex in a 1:1 acetonitrile/buffer mixture, using the same solution conditions as those employed for kinetic studies. Using a model with four protonation equilibria[47] (Scheme 1) yielded the best fit to the data, with the four pK_a values given in Table 3. pK_{a4} (7.53) corresponds to the second catalytically relevant pK_a determined from the phosphatase kinetics, while pK_{a2} (4.13) is similar to the first pK_a determined kinetically. In fact, these pK_a's are in reasonable good agreement with those determined from spectrophotometric titration experiments of the $[Fe^{III}Fe^{II}\mathbf{L1}(\mu\text{-}OAc)_2]^+$ complex and also show the expected trends when compared to the pK_a values of the corresponding oxidized $Fe^{III}Fe^{III}$ complex.[4] On the other hand, deprotonation of the bridging OH^- with the formation of a $Fe^{III}(\mu\text{-}O)Fe^{II}$ species was unexpected given that the isostructural $Fe^{III}M^{II}$ (M^{II} = Cu, Zn, Ni, and Co) complexes do not show this process. Nevertheless, on the basis of the experimental results presented in this study, at present we do not have a reasonable explanation for the distinct behavior of the $[Fe^{III}Fe^{II}\mathbf{L1}(\mu\text{-}OAc)_2]^+$ complex. Finally, it should be noted that the pK_a's obtained from the kinetic data are related to the protonation equilibrium involving the catalyst–substrate complex, while the corresponding lower pK_a of 4.13 is associated with the free catalyst. Thus, differences between these pK_a's should be expected. Mechanistic implications of the assignment of these equilibria are described in the Solution and Phosphoester Hydrolytic Properties section of the Discussion.

Protein Hydrolysis. The catalytic promiscuity already reported for $[Fe^{III}Fe^{II}\mathbf{L1}(\mu\text{-}OAc)_2]^+$, due its catecholase-like activity and DNA cleavage properties,[4] encouraged us to extend the list of substrates and reactions catalyzed by the title compound. In this context, an aqueous solution of $[Fe^{III}Fe^{II}\mathbf{L1}(\mu\text{-}OAc)_2]^+$ was assessed for its ability to cleave proteins such as BSA. The results from protein cleavage assays are shown in Figure 9.

In the absence of $[Fe^{III}Fe^{II}\mathbf{L1}(\mu\text{-}OAc)_2]^+$, the amount of BSA remains unchanged during the 25 h of reaction. In the presence of $[Fe^{III}Fe^{II}\mathbf{L1}(\mu\text{-}OAc)_2]^+$, however, the amount of intact BSA was decreased over the time of the reaction, which suggests fragmentation of the protein into indistinguishably small fragments. After 25 h, the amount of BSA dropped ~40%. Under these reaction conditions, the rate of BSA fragmentation could be estimated as 3.29×10^{-2} h^{-1}, a rate constant comparable to those of other metal complexes with proteolytic activity and under similar reaction conditions.[57,58] This rate corresponds to a protein half-life of ~21 h. Under the same conditions, it was not possible to determine the rate of the corresponding uncatalyzed reaction. The results presented here suggest that aqueous solutions of $[Fe^{III}Fe^{II}\mathbf{L1}(\mu\text{-}OAc)_2]^+$ can cleave not only DNA[4] but also proteins. Similar behavior was also reported by Oliveira and co-workers, who demonstrated that a mononuclear copper(II) phenolate complex was able to hydrolyze both BSA[30] and DNA.[59] An interesting property of the aqueous solutions of $[Fe^{III}Fe^{II}\mathbf{L1}(\mu\text{-}OAc)_2]^+$ is their ability to cleave proteins at mild incubation conditions (pH 6 and 37 °C), different from those of other metal complexes, which have similar activity with reaction optima at extreme pH values (below 4.0 or above 9.0) and high temperatures (above 50 °C).

dx.doi.org/10.1021/ic201711p | Inorg. Chem. 2012, 51, 2065–2078

Scheme 1. Proposed Solution Equilibria for $[Fe^{III}Fe^{II}L1(\mu\text{-}OAc)_2]^+$

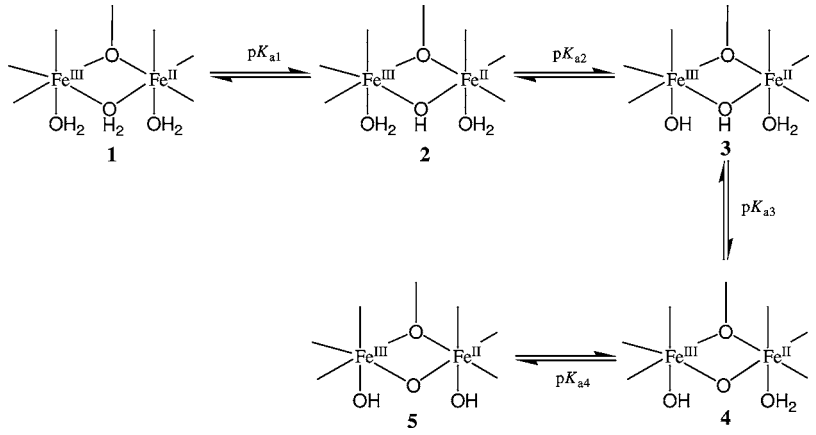

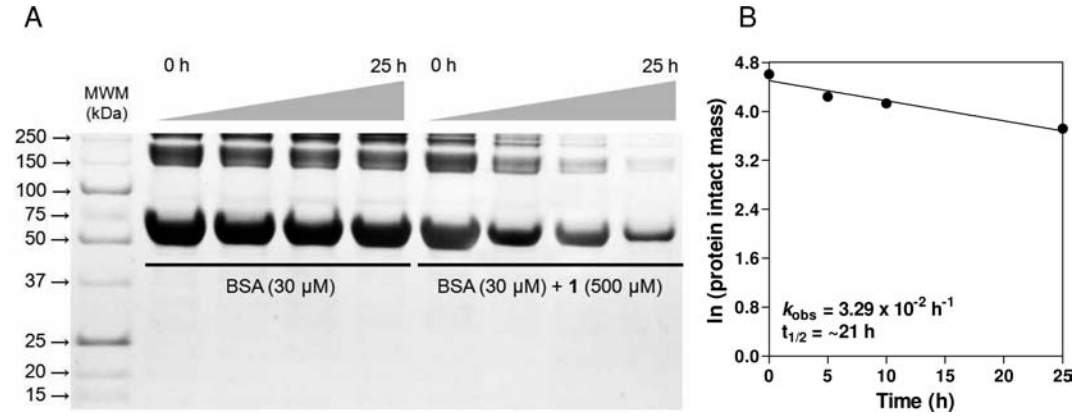

Figure 9. Cleavage of BSA promoted by an aqueous solution of $[Fe^{III}Fe^{II}\mathbf{L1}(\mu\text{-}OAc)_2]^+$ over 25 h of reaction (A). Kinetic analysis of BSA cleavage (B). Assay conditions: [BSA] = 30 μmol L^{-1}; $[Fe^{III}Fe^{II}\mathbf{L1}(\mu\text{-}OAc)_2]^+$ = 500 μmol L^{-1}; [MES, pH 6.0] = 10 mmol L^{-1}; [NaCl] = 10 mmol L^{-1}; temperature = 37 °C; reaction times = 0, 5, 10, and 25 h.

Analysis of BSA by MALDI-TOF MS revealed a major peak (m/z 66 541 ± 256) in agreement with the theoretical intact mass of BSA (66 432.96), as expected. Protein samples that were allowed to react with a solution of $[Fe^{III}Fe^{II}\mathbf{L1}(\mu\text{-}OAc)_2]^+$ for 5, 10, and 25 h (Figure S3 in the Supporting Information) showed a molecular mass increase of 588 ± 104 Da in the major peak of BSA that may be related to the binding of the complex to the protein. Maity and co-workers,[60] Roy and co-workers,[61] and ourselves[59] using a similar technique demonstrated that different metal complexes may lead to a decrease in the BSA major peak intensity, the appearance of other peaks relative to BSA fragmentation, or simply a BSA increase in mass due to complex binding.

CD is a useful technique to investigate changes in the secondary structure in proteins mediated by small molecules.[62] BSA has a high percentage of α-helix in its structure, presenting a very characteristic CD spectrum with two strong negative bands at 209 and 220 nm.[63] We observed a decrease of these two negative bands when the protein sample is titrated with aqueous solutions of $[Fe^{III}Fe^{II}\mathbf{L1}(\mu\text{-}OAc)_2]^+$ (Figure S4 in the Supporting Information). This effect suggests that the interaction of aqueous solutions of $[Fe^{III}Fe^{II}\mathbf{L1}(\mu\text{-}OAc)_2]^+$ with BSA leads to a disruption in the secondary structure of the protein, most probably in its α-helix content. Similar effects were already reported by Xu and colleagues[64] and Toneatto and Argüello[65] for other metal complexes.

DISCUSSION

Geometric and Electronic Structures of $[Fe^{III}Fe^{II}L1(\mu\text{-}OAc)_2]^+$. In the solid state, the X-ray crystallographic structure of the complex cation $[Fe^{III}Fe^{II}\mathbf{L1}(\mu\text{-}OAc)_2]^+$ is very similar to that reported previously as a perchlorate salt and the isostructural $Fe^{III}M^{II}$ (M = Cu^{II}, Mn^{II}, Ni^{II}, and Co^{II}) complexes. The electronic structure calculations reveal that the weak antiferromagnetic exchange coupling is mediated by the phenoxo bridge and further that there is significant electron density on the terminal iron(III) phenolate O atom. In solution, as judged by MS, the bridging acetate ligands may be either intact (acetonitrile), partially dissociated (MeOH), or completely dissociated [acetonitrile/buffer (50:50)].

MCD Spectroscopy. Yang et al.[43] reported an extensive MCD study of reduced uteroferrin both unligated and in the presence of phosphate and molybdate. Spectra were measured in both the visible (CT) and NIR regions (d−d transitions). On the basis of a comparison with model data, the weak ferric d−d transitions indicated that this metal ion may be six-coordinate, in contrast with an ENDOR study,[66] which indicated that no terminal H_2O was located on the Fe^{III}. The nominal e_g−t_{2g} splitting of the d−d orbitals (11 000 cm^{-1}) was determined[67] from Gaussian resolution (five bands) of the absorption spectrum in the CT region.

The MCD spectrum of the model complex is qualitatively similar to that of the enzyme, specifically, the phenolate-to-Fe^{III} LMCT band that is prominent at ∼550 nm. However, the

dx.doi.org/10.1021/ic201711p | Inorg. Chem. 2012, 51, 2065−2078

strong negative band at ~400 nm is not observed in uteroferrin and is attributed to an Fe^{II}-to-pyridine metal-to-ligand CT. Transitions of this type have been observed at similar energies in a range of other complexes.[68,69] For example, the $Ga^{III}Fe^{II}$ complex with a ligand similar to **L1** shows such a transition at 387 nm.[39] The higher-energy transitions are far less resolved than those in uteroferrin, precluding determination of the value of the ligand-field splitting in this manner. The MCD bands in the IR region at 11 370 and 12 150 cm^{-1} likely correspond to the ligand-field bands of the Fe^{III} center, indicating that similar ligand-field strengths (11 000 vs 11 370 cm^{-1}) at the Fe^{III} site are exhibited in both the model complex and enzyme. The precise energies of these bands are ambiguous, given that there is no detectable absorbance or CD intensity to confirm the band positions. The broad transition at ~8000 cm^{-1} could be attributed to either an intervalence CT or a d−d transition from the six-coordinate Fe^{II} center.[43]

Uteroferrin also shows no unusual temperature-dependent band such as that observed at 428 nm in the model complex. On the basis of the energy of this band, it is also likely attributable to a pyridine-to-Fe^{II} CT,[68,69] likely originating from the $S = {}^3/_2$ state of the exchange-coupled multiplet. In uteroferrin, VT MCD data were analyzed by Yang et al.[43] to determine the coupling of the active site ($|-J| > 6$ cm^{-1}). The presence of phosphate, but not molybdate, perturbed the bridging between the metal ions, resulting in a decreased coupling constant and a red shift of the CT band. This is indicative of a weakening of the μ-OH−Fe^{III} bond and a compensatory increase in the strength of the Fe^{III}−Tyr bond.[43]

For the model complex, the exchange coupling has also been determined from the MCD; analysis of the VT MCD gives a J of −3.4 cm^{-1}, while fitting the area of the excited band to the Boltzmann distribution for $S_{tot} = {}^3/_2$ results in a J of −5.6 cm^{-1}. These values compare reasonably with the previously reported exchange coupling constant for $[Fe^{III}Fe^{II}\mathbf{L1}(\mu\text{-OAc})_2]^+$ (−7.4 cm^{-1}) obtained from magnetic susceptibility measurements[3] and are also similar to the values obtained from the MCD of uteroferrin.[43] The reduction of the J value for $[Fe^{III}Fe^{II}\mathbf{L1}(\mu\text{-OAc})_2]^+$ in solution (−5.6 cm^{-1}) compared to the solid-state value (−7.4 cm^{-1}) may indicate that the geometry of the dimer has relaxed such that the metal−metal distance has increased.

EPR Spectroscopy. The failure to observe a resolved EPR signal corresponding to an $Fe^{III}Fe^{II}$ species except at very low (<2 K) temperature is somewhat unusual: antiferromagnetically coupled $Fe^{III}Fe^{II}$ systems typically exhibit EPR spectra with $g_{eff} < 2$, and spectra have been observed in both complexes[11,70−73] and in a range of enzymes,[42,74−82] including mammalian PAPs.[45,83−87] However, similar phenoxo-bridged $Fe^{III}Fe^{II}$ complexes[7,67] also display no or unresolved EPR signals at low temperatures. This may be attributed to the fact that the exchange interaction J and the ZFS parameter D of the Fe^{II} ion are of similar magnitude. Indeed, Lambert et al.[7] reported a J/D ratio of 4:13 for the similar complex $[Fe^{III}Fe^{II}(BPHPMP)(mpdp)](BPh_4)$ [H_2BPHPMP = 2-[*N*,*N*-bis(2-methylpyridyl)-aminomethyl]-6-[*N*-(2-hydroxyphenyl)-*N*-(2-pyridylmethyl)-aminomethyl]-4-methylphenol; mpdp = 1,3-benzenedipropionate] in which no EPR spectrum was detected. When the exchange interaction J and the ZFS parameter D are of similar magnitude, the g values become very sensitive to variations of the ZFS parameters arising from heterogeneities in the microenvironment. This results in a significant increase in the effective g strain and anisotropy, leading to very broad and difficult to detect EPR resonances.[83] In addition, the presence of closely lying excited states will induce rapid relaxation through Orbach relaxation,[44] resulting in an apparent EPR-silent spectrum.

The formation of a binuclear diiron(III) phosphate complex upon the addition of phosphate to the complex in methanol is supported by MS and is particularly pertinent in light of the fact that uteroferrin is also more readily oxidized upon phosphate binding.[5,6,88−90] Relatively few EPR investigations of binuclear Fe^{III} systems have been reported.[48,56,91−94] Typically, the ions are coupled by μ-oxo bridges, mediating very strong antiferromagnetic exchange coupling resulting in a diamagnetic ($S_{tot} = 0$) ground state, predominant even at high temperatures.[82,95] Several complexes with EPR spectra similar to that observed here have been reported, but they typically only show population of the excited states at much higher temperatures, indicating a stronger exchange coupling than is observed in this case.[91−93]

Several of the previously reported spectra have been simulated as combinations of $S_{tot} = 1$, 2, and 3 spin states.[56,91−93] However, the spin projection factors for the magnitude of the axial ZFS in $S_1 = S_2 = {}^5/_2$ systems indicate that $S_{tot} = 3$ is the spin state most likely to give rise to resolved transitions in the presence of strain broadening.[48] Indeed, simulation of the observed spectrum as a $S_{tot} = 3$ spin state satisfactorily reproduced the experimentally observed resonances, with the simulation significantly improved by the introduction of a higher order B_4^0 ZFS term. This term accounts for mixing between spin functions of the ground and excited exchange multiplets induced by anisotropic second-order dipole−dipole coupling terms in the spin Hamiltonian.[96−98]

Also of note is the weaker exchange coupling of the phosphate-bound oxidized complex, $J \sim -3.5$ cm^{-1}, in contrast to the value of ~−5 cm^{-1} for the $Fe^{III}Fe^{II}$ species. Interestingly, in bovine spleen PAP, the phosphate-bound oxidized enzyme also has a weaker coupling than that of the reduced enzyme.[99] In similar alkoxo-bridged Fe^{III}_2 complexes, magnetic susceptibility has also indicated the presence of weak antiferromagnetic coupling ($0 > J > -5$ cm^{-1}).[100,101]

Solution and Phosphoester Hydrolytic Properties. The process of acetate/diphenylphosphate exchange on the Fe^{III}−Fe^{II} center has been studied previously, and it was found that acetate ligands are readily displaced by diphenylphosphate (dpp^-) in both the heterovalent and diferric states of the complex. Indeed, MS results presented herein show that in acetonitrile the $[Fe^{III}Fe^{II}\mathbf{L1}(\mu\text{-OAc})_2]^+$ complex cation is intact, although in a acetonitrile/buffer (50:50) solution, the bridging acetate ligands are lost. Ligand exchange in the diferric complex is concomitant with a reduction to the mixed-valent state, where the liberated acetate is proposed as the reducing agent.[102] These observations have potential ramifications for the kinetic activity of the complexes because it is clearly important that at least one of the bridging acetates must be displaced by the solvent system employed, leaving sites available for phosphate binding and subsequent phosphorolysis.

Of the pK_a values given in Table 1, two are catalytically relevant. Although the potentiometric (4.13) and kinetic (5.03) values of pK_{a2} are somewhat different, this can be understood in terms of the kinetics probing the pK_a of the complex−substrate species. Moreover, the MS spectrum recorded in 50:50 acetonitrile/H_2O indicates that the bound acetates are displaced under these conditions, as expected.

dx.doi.org/10.1021/ic201711p | *Inorg. Chem.* 2012, 51, 2065−2078

Table 4. pK_a's and Kinetic Parameters for L1 Complexes

complex	kinetic pK_a	potentiometric pK_a	$k_{cat} \times 10^4$ (s^{-1})	K_m (mmol L^{-1})	pH optimum
$[Fe^{III}Fe^{II}\mathbf{L1}(\mu\text{-OAc})_2](BF_4)$	5.03, 6.92	3.02, 4.13, 5.76, 7.53	18.8	4.63	5.6
$[Fe^{III}Cu^{II}\mathbf{L1}(\mu\text{-OAc})_2](ClO_4)$[103]	5.2, 8.5	5.25, 6.20, 7.82	18.0	11	7
$[Fe^{III}Mn^{II}\mathbf{L1}(\mu\text{-OAc})_2](ClO_4)$[108]			7.1	2.1	6.7
$[Fe^{III}Ni^{II}\mathbf{L1}(\mu\text{-OAc})_2](ClO_4)$[28]	4.91, 8.34	5.30, 6.80, 8.61	4.4	3.8	6
$[Fe^{III}Zn^{II}\mathbf{L1}(\mu\text{-OAc})_2](ClO_4)$[114]	4.80, 7.50	4.86, 6.00, 7.22	11.0	8.1	6.1
$[Ga^{III}Zn^{II}\mathbf{L1}(\mu\text{-OAc})_2](ClO_4)$[115]	5.35, 8.55	5.59, 6.19, 7.96	14.0	7.1	6.8
$[Fe^{III}Zn^{II}\mathbf{L1}(\mu\text{-OH})](ClO_4)_2$[107]	5.3, 8.1	2.93, 4.81, 8.30	9.13	4.2	6.5
$[Fe^{III}Co^{II}\mathbf{L1}(\mu\text{-OAc})_2](ClO_4)$[55]	5.2, 8.8	5.0, 6.58, 8.31	14.2	92.7	7.0
$[Ga^{III}Co^{II}\mathbf{L1}(\mu\text{-OAc})_2](ClO_4)$[55]	5.7, 8.9	5.46, 6.57, 8.30	18.7	88.1	7.5

These catalytically relevant pK_a values (i.e., pK_{a2} and pK_{a4}) are readily assigned based on the pH dependence of the kinetic properties of isostructural complexes. The pK_a values of Fe^{III}-H_2O deprotonation for mixed-valence $M^{III}M^{II}$ complexes with the same ligand are typically in the range of 4.6−5.2.[28,55,103,104] Thus, pK_{a2} is assigned to a terminal, Fe^{III}-bound H_2O, also in good agreement with the pK_{es1} of uteroferrin of 4.15.[105] The second catalytically relevant pK_{a4} of 6.93 is assigned to deprotonation of a H_2O molecule bound to the divalent metal ion, which is in the range of values (6.8−8.0) found for the corresponding $Fe^{III}M^{II}$ complexes (M^{II} = Ni, Zn, and Mn).[104]

Whereas pK_{a2} and pK_{a4} correspond to deprotonation of Fe^{III}-H_2O and Fe^{II}-H_2O, respectively, the assignments of pK_{a1} and pK_{a3} are more difficult. On the basis of its acidity and by comparison with the enzyme[106] and other relevant systems,[29,107] pK_{a1} is assigned to a metal-ion-bridging H_2O molecule. In the isostructural systems, deprotonation of the bridging H_2O has not been observed. However, this may be due to the use of a different solvent system (ethanol/H_2O), and no measurement below pH 4 with this solvent system was attempted.[28,108] However, when the similar system $[Fe^{III}(H_2O)(\mu\text{-OH})Zn(II)\mathbf{L1}]^{2+}$ was titrated in a H_2O/acetonitrile solvent system between pH 2 and 10, a pK_a of 2.93 was observed and assigned to deprotonation of a bridging H_2O ligand, in good agreement with the value found for $[Fe^{III}Fe^{II}\mathbf{L1}(\mu\text{-OAc})_2]^+$ (3.02).[107] In a H_2O-bridged Ni_2 complex, a pK_a of 4.4 for the bridging H_2O was determined potentiometrically.[109] Replacement of one of the divalent metal ions with a trivalent metal ion could plausibly decrease this pK_a by 1−2 orders of magnitude, suggesting that the assignment of pK_{a1} to deprotonation of a bridging H_2O is reasonable.[110]

pK_{a3} is then attributed to deprotonation of the bridging hydroxide to a μ-oxo. This process is presumably not catalytically relevant (vide supra). Literature values of pK_a's for deprotonation of μ-hydroxo ligands in Fe^{III}_2 complexes range from 2 to 4.3.[111−113] Replacement of one trivalent Fe with a divalent Fe could plausibly increase this value by several orders of magnitude, consistent with the observed value of pK_{a3} of 5.76 when compared to the corresponding pK_a of 4.22 observed in the oxidized $Fe^{III}Fe^{III}$ complex. In the isostructural $Fe^{III}M^{II}$ complexes (M = Cu, Fe, Zn, and Ni; Table 4), this pK_a has been assigned to deprotonation of a second Fe^{III}-H_2O moiety, which, upon deprotonation, forms a μ-hydroxo species. In the current situation, however, such an assignment is inappropriate given that there is already a μ-hydroxo bridge. In the $Fe^{III}Zn^{II}(\mu\text{-OH})$ complex, no corresponding pK_a was observed.[107] Furthermore, the MS spectrum of the complex under kinetic conditions supports the possibility of formation of an oxo species, at least under the conditions of the MS.

On the basis of the above assignments, Scheme 1 shows the proposed structures for the species corresponding to each protonation equilibrium. The catalytic parameters of the current complex are readily comparable to those of the isostructural complexes, with the observed $k_{cat.}$ for a solution of $[Fe^{III}Fe^{II}\mathbf{L1}(\mu\text{-OAc})_2]^+$ being one of the highest within the investigated series of mixed-valence complexes (Table 4). A comparison of the potentiometrically and kinetically determined pK_a values and assignment of the values to protonation equilibria offer insight into the speciation of the complex and the kinetically active species. On the basis of analysis of the pH dependence of $[Fe^{III}Fe^{II}\mathbf{L1}(\mu\text{-OAc})_2]^+$, the activity of the complex is increased by the protonation event corresponding to pK_{a2} and decreased by that corresponding to pK_{a4}. Figure 10

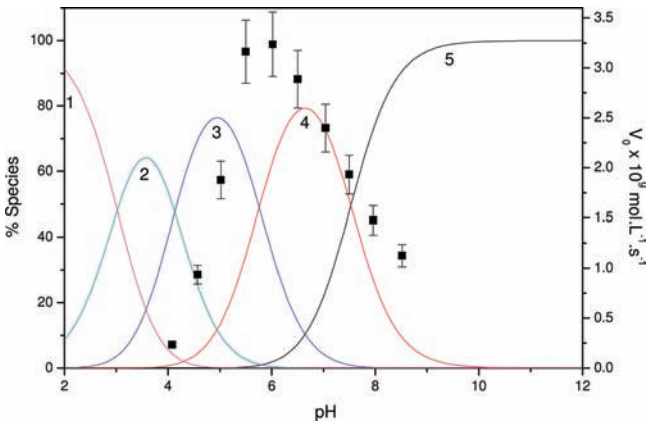

Figure 10. Rate of BDNPP hydrolysis by $[Fe^{III}Fe^{II}\mathbf{L1}(\mu\text{-OAc})_2]^+$ superimposed on the speciation plot obtained from the potentiometric titration (species labels refer to Scheme 1).

shows the correspondence of the kinetic and potentiometric speciation.

The kinetic species clearly corresponds to the sum of species **3** and **4**, with pK_{a3} having no impact catalytically. That is, deprotonation of the Fe^{III}-bound H_2O results in an increase in the catalytic activity, while deprotonation of the Fe^{II}-bound H_2O results in a decrease in the catalytic activity and deprotonation of the bridging hydroxide has no impact upon the catalysis.

On the basis of the experimental data discussed above and the mechanism proposed by Lanznaster et al.[114] for the isostructural $Fe^{III}Zn^{II}$ complex, a mechanism similar to that shown in Scheme 2 is proposed for $Fe^{III}Fe^{II}\mathbf{L1}(\mu\text{-OAc})_2]^+$.

The activity profile along with the kinetic isotope effect observed in hydrolysis of the diester and the lack of activity in

dx.doi.org/10.1021/ic201711p | Inorg. Chem. 2012, 51, 2065−2078

Scheme 2. Mechanism for Hydrolysis of BDNPP by in an Aqueous Solution of $[Fe^{III}Fe^{II}L1(\mu\text{-}OAc)_2]^+$

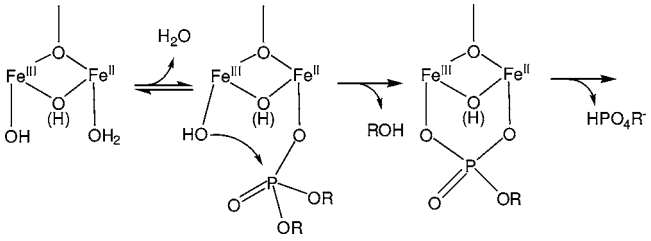

hydrolysis of the monoester by the catalyst $[Fe^{III}Fe^{II}L1(\mu\text{-}OAc)_2]^+$ demonstrate that Fe^{III}-OH is the likely reaction-initiating nucleophile rather than a bridging hydroxide and that the substrate binds at the divalent metal ion, similar to the PAPs.[115,116] Hydrolysis would result in a bridging coordination mode of the bound monoester, also similar to that proposed for PAPs. The decrease in the activity upon deprotonation of Fe^{II}-H_2O indicates that the substrate is replacing the bound H_2O. Hydroxide would be less labile than an aqua ligand, resulting in less facile substrate binding. The fully deprotonated species maintains a level of activity that is approximately 10% of the maximum value, suggesting that some ligand exchange on the divalent metal ion of species **5** remains possible. Such a mechanism is similar to that proposed for some PAPs, in particular uteroferrin, red kidney bean, and bovine spleen PAPs,[117−119] although recent stopped-flow measurements indicated that, at least in uteroferrin, two nucleophiles are present, one being in a metal-ion-bridging position and the other in the second coordination sphere, activated via hydrogen-bond interactions with a Fe^{III}-bound hydroxide and amino acid side chains in the substrate binding pocket.[120]

Protein Hydrolytic Properties. The results presented here suggest that aqueous solutions of $[Fe^{III}Fe^{II}L1(\mu\text{-}OAc)_2]^+$ bind and subsequently cleave BSA into indistinguishably small fragments. MALDI-TOF MS analysis was performed and binding to BSA was indeed confirmed by an increase in the molecular mass of intact BSA due to complex binding. By CD analysis, it was possible to infer that aqueous solutions of $[Fe^{III}Fe^{II}L1(\mu\text{-}OAc)_2]^+$ bind to BSA, inducing a decrease in the α-helical structure content of the protein. We are undertaking further investigations to identify the putative site(s) of hydrolysis.

CONCLUSIONS

The Fe_2 model complex $[Fe^{III}Fe^{II}L1(\mu\text{-}OAc)_2]^+$ is a good spectroscopic model for uteroferrin. The MCD spectrum of the complex is similar to that of the enzyme, the exchange coupling determined by MCD compares well to the weak antiferromagnetic coupling of the enzyme, and oxidation of the complex in the presence of phosphate gives rise to a complex EPR spectrum that mimics accurately the change in the redox potential of the enzyme when in the presence of phosphate. The reduction in the strength of the exchange coupling of the oxidized enzyme with phosphate bound compared to the reduced enzyme is also reproduced in the model system. Additionally, the model serves as a functional model for the PAPs, and the elucidated mechanism for hydrolysis of the activated substrate BDNPP follows one of the proposed pathways for enzymatic catalysis: binding of the substrate to the divalent metal ion, with a terminally Fe^{III}-bound hydroxide serving as the nucleophile. The complex is, therefore, both a functionally and structurally relevant model of the active site of the PAPs. Finally, the catalytic promiscuity, already attributed to aqueous solutions of $[Fe^{III}Fe^{II}L1(\mu\text{-}OAc)_2]^+$, was extended by showing that this complex is also capable of cleaving proteins under mild experimental conditions (pH 6.0 and 37 °C).

ASSOCIATED CONTENT

Supporting Information

Tables S1−S4 and Figures S1−S6, crystallographic data in CIF format, and computational chemistry files. This material is available free of charge via the Internet at http://pubs.acs.org. Also, crystallographic data (without structure factors) for the structure reported in this paper have been deposited with the Cambridge Crystallographic Data Centre as supplementary publication number CCDC 837263. Copies of the data can be obtained free of charge from the CCDC [12 Union Road, Cambridge CB2 1EZ, U.K.; phone (+44) 223-336-408; fax (+44) 1223-336-003; e-mail deposit@ccdc.cam.ac.uk; Web site www.ccdc.cam.ac.uk].

AUTHOR INFORMATION

Corresponding Author

*E-mail: m.riley@uq.edu.au (M.J.R.), ademir@qmc.ufsc.br (A.N.). Telephone: ++61 7 3365 3932 (M.J.R.), ++55 48 3721 6844 (A.N.). Fax: ++61 7 3365 4299 (M.J.R.), ++55 48 3721 9711 (A.N.).

ACKNOWLEDGMENTS

The authors thank CNPq, CAPES, PROCAD, FAPESC, and INCT-Catálise (Brazil) and the Australian Research Council (Grant DP0986292) for financial support and the National Computational Infrastructure for access to supercomputer facilities at the Australian National University.

DEDICATION

This paper is dedicated to Prof. Karl Wieghardt on the occasion of his retirement.

REFERENCES

(1) Mitic, N.; Smith, S. J.; Neves, A.; Guddat, L. W.; Gahan, L. R.; Schenk, G. *Chem. Rev.* **2006**, *106*, 3338−3363.
(2) Guddat, L. W.; McAlpine, A. A.; Hume, D. A.; Hamilton, S.; de Jersey, J.; Martin, J. L. *Structure* **1999**, *7*, 757−767.
(3) Neves, A.; de Brito, M. A.; Drago, V.; Griesar, K.; Haase, W. *Inorg. Chim. Acta* **1995**, *237*, 131−135.
(4) Neves, A.; Bortoluzzi, A. J.; Jovito, R.; Peralta, R. A.; de Souza, B.; Szpoganicz, B.; Joussef, A. C.; Terenzi, H.; Severino, P. C.; Fischer, F. L.; Schenk, G.; Riley, M. J.; Smith, S. J.; Gahan, L. R. *J. Braz. Chem. Soc.* **2010**, *21*, 1201−1212.
(5) Bernhardt, P. V.; Schenk, G.; Wilson, G. J. *Biochemistry* **2004**, *43*, 10387−10392.
(6) Wang, D. L.; Holz, R. C.; David, S. S.; Que, L.; Stankovich, M. T. *Biochemistry* **1991**, *30*, 8187−8194.
(7) Lambert, E.; Chabut, B.; Chardon-Noblat, S.; Deronzier, A.; Chottard, G.; Bousseksou, A.; Tuchagues, J.-P.; Laugier, J.; Bardet, M.; Latour, J.-M. *J. Am. Chem. Soc.* **1997**, *119*, 9424−9437.
(8) Bernard, E.; Moneta, W.; Laugier, J.; Chardon-Noblat, S.; Deronzier, A.; Tuchagues, J.-P.; Latour, J.-M. *Angew. Chem., Int. Ed.* **1994**, *33*, 887−889.
(9) Chardon-Noblat, S.; Horner, O.; Chabut, B.; Avenier, F.; Debaecker, N.; Jones, P.; Pecaut, J.; Dubois, L.; Jeandey, C.; Oddou, J.-L.; Deronzier, A.; Latour, J.-M. *Inorg. Chem.* **2004**, *43*, 1638−1639.

(10) Suzuki, M.; Oshio, H.; Uehara, A.; Endo, K.; Yanaga, M.; Kida, S.; Saito, K. *Bull. Chem. Soc. Jpn.* **1988**, *61*, 3907−3913.
(11) Suzuki, M.; Uehara, A.; Oshio, H.; Endo, K.; Yanaga, M.; Kida, S.; Saito, K. *Bull. Chem. Soc. Jpn.* **1987**, *60*, 3547−3555.
(12) *Amsterdam Density Functional, Scientific Computing and Modelling*; Theoretical Chemistry, Vrije Universiteit: Amsterdam, The Netherlands (http://www.scm.com).
(13) Fonseca Guerra, C.; Snijders, J. G.; te Velde, G.; Baerends, E. J. *Theor. Chem. Acc.* **1998**, *99*, 391−403.
(14) te Velde, G.; Bickelhaupt, F. M.; van Gisbergen, S. J. A.; Fonseca Guerra, C.; Baerends, E. J.; Snijders, J. G.; Ziegler, T. *J. Comput. Chem.* **2001**, *22*, 931−967.
(15) van Lenthe, E.; Baerends, E. J.; Snijders, J. G. *J. Chem. Phys.* **1993**, *99*, 4597.
(16) van Lenthe, E.; Baerends, E. J.; Snijders, J. G. *J. Chem. Phys.* **1994**, *101*, 9783.
(17) van Lenthe, E.; Ehlers, A. E.; Baerends, E. J. *J. Chem. Phys.* **1999**, *110*, 8943.
(18) Pye, C. C.; Ziegler, T. *Theor. Chem. Acc.* **1999**, *101*, 396−408.
(19) Adamo, C.; Barone, V. *J. Chem. Phys.* **1999**, *110*, 6158.
(20) Ernzerhof, M.; Scuseria, G. *J. Chem. Phys.* **1999**, *110*, 5029.
(21) Perdew, J. P.; Burke, K.; Ernzerhof, M. *Phys. Rev. Lett.* **1996**, *77*, 3865.
(22) van Gisbergen, S. J. A.; Snijders, J. G.; Baerends, E. J. *Comput. Phys. Commun.* **1999**, *118*, 119.
(23) Gritsenko, O. V.; Schipper, P. R. T.; Baerends, E. J. *Chem. Phys. Lett.* **1999**, *302*, 199.
(24) Hanson, G. R.; Noble, C. J.; Benson, S. In *Biological magnetic resonance. High resolution EPR: applications to metalloenzymes and metals in medicine*; Hanson, G. R., Berliner, L. J., Eds.; Springer: New York, 2009; pp 105−173.
(25) Riley, M. J.; Krausz, E. R.; Stanco, A. *J. Inorg. Biochem.* **2003**, *96*, 217.
(26) Neves, A.; Erthal, S. M. D.; Vencato, I.; Ceccato, A. S.; Mascarenhas, Y. P.; Nascimento, O. R.; Hörner, M.; Batista, A. A. *Inorg. Chem.* **1992**, *31*, 4749−4755.
(27) Bunton, C. A.; Farber, S. J. *J. Org. Chem.* **1969**, *34*, 767.
(28) Batista, S. C.; Neves, A.; Bortoluzzi, A. J.; Vencato, I.; Peralta, R. A.; Szpoganicz, B.; Aires, V. V. E.; Terenzi, H.; Severino, P. C. *Inorg. Chem. Commun.* **2003**, *6*, 1161−1165.
(29) Peralta, R. A.; Bortoluzzi, A. J.; Souza, B.; Jovito, R.; Xavier, F. R.; Couto, R. A. A.; Casellato, A.; Nome, F.; Dick, A.; Gahan, L. R.; Schenk, G.; Hanson, G. R.; de Paula, C. S.; Pereira-Maia, E. C.; Machado, S. d. P.; Severino, P. C.; Pich, C. T.; Bortolotto, T.; Terenzi, H.; Castellano, E. E.; Neves, A.; Riley, M. J. *Inorg. Chem.* **2010**, *49*, 11421−11438.
(30) Oliveira, M. C. B.; Scarpellini, M.; Neves, A.; Terenzi, H.; Bortoluzzi, A. J.; Szpoganicz, B.; Greatti, A.; Mangrich, A. S.; De Souza, E. M.; Fernandez, P. M.; Soares, M. R. *Inorg. Chem.* **2005**, *44*, 921−929.
(31) Brown, I. D.; Altermatt, D. *Acta Crystallogr.* **1985**, *B41*, 244−247.
(32) Paim, L. A.; Augusti, D. V.; Dalmazio, I.; Alves, T.; Augusti, R.; Siebald, H. G. L. *Polyhedron* **2005**, *24*, 1153−1159.
(33) Blades, A. T.; Ikonomou, M. G.; Kebarle, P. *Anal. Chem.* **1991**, *63*, 2109−2114.
(34) Andersen, U. N.; McKenzie, C. J.; Bojesen, G. *Inorg. Chem.* **1995**, *34*, 1435−1439.
(35) Budimir, N.; Fournier, F.; Bailly, T.; Burgada, R.; Tabet, J.-C. *Rapid Commun. Mass Spectrom.* **2005**, *19*, 1822−1828.
(36) Di Marco, V. B.; Bombi, G. G. *Mass Spectrom. Rev.* **2006**, *25*, 347−379.
(37) Neves, A.; Terenzi, H.; Peralta, R. A.; Severino, P. C. Bioinspired Synthetic Analogues for Purple Acid Phosphatases and Catalytic Promiscuity. In *Molecular and Supramolecular Bioinorganic Chemistry: Applications in Medical and Environmental Sciences*; Mercê, A. L. R. F. J., Recio, M. Á. L., Eds.; Nova Science Publishers: New York, 2011; Vol. 2, pp 31−71.
(38) Neves, A.; de Brito, M. A.; Vencato, I.; Drago, V.; Griesar, K.; Haase, W. *Inorg. Chem.* **1996**, *35*, 2360−2368.
(39) Borovik, A. S.; Papaefthymiou, V.; Taylor, L. F.; Anderson, O. P.; Que, L. Jr. *J. Am. Chem. Soc.* **1989**, *111*, 6183−6195.
(40) Pyrz, J. W.; Sage, J. T.; Debrunner, P. G.; Que, L. Jr. *J. Biol. Chem.* **1986**, *261*, 11015−11020.
(41) Owen, J. *J. Appl. Phys.* **1961**, *32*, S213−S217.
(42) McCormick, J. M.; Reem, R. C.; Solomon, E. I. *J. Am. Chem. Soc.* **1991**, *113*, 9066−9079.
(43) Yang, Y.-S.; McCormick, J. M.; Solomon, E. I. *J. Am. Chem. Soc.* **1997**, *119*, 11832−11842.
(44) Pilbrow, J. R. *Transition Ion Electron Paramagnetic Resonance*; Clarendon Press: Oxford, U.K., 1990.
(45) Averill, B. A.; Davis, J. C.; Burman, S.; Zirino, T.; Sanders-Loehr, J.; Loehr, T. M.; Sage, J. T.; Debrunner, P. G. *J. Am. Chem. Soc.* **1987**, *109*, 3760−3767.
(46) Bencini, A.; Gatteschi, D. *Electron Paramagnetic Resonance of Exchange Coupled Systems*; Springer-Verlag: Heidelberg, Germany, 1990.
(47) Gans, P.; Sabatini, A.; Vacca, A. *J. Chem. Soc., Dalton Trans.* **1985**, 1195−1200.
(48) Bill, E.; Beckmann, U.; Wieghardt, K. *Hyperfine Interact.* **2002**, *144*, 183−198.
(49) ter Heerdt, P.; Stefan, M.; Goovaerts, E.; Caneschi, A.; Cornia, A. *J. Magn. Reson.* **2006**, *179*, 29−37.
(50) Golombek, A. P.; Hendrich, M. P. *J. Magn. Reson.* **2003**, *165*, 33−48.
(51) Epel, B.; Schaefer, K. O.; Quentmeier, A.; Friedrich, C.; Lubitz, W. *J. Biol. Inorg. Chem.* **2005**, *10*, 636−642.
(52) Noodleman, L. *Chem. Phys.* **1981**, *74*, 5737.
(53) Delfs, C. D.; Stranger, R. *Inorg. Chem.* **2001**, *40*, 3061.
(54) Kantacha, A.; Buchholz, R.; Smith, S. J.; Schenk, G.; Gahan, L. R. *J. Biol. Inorg. Chem.* **2011**, *15*, 25−32.
(55) Xavier, F. R.; Neves, A.; Casellato, A.; Pereira-Maia, E. C.; Bortoluzzi, A. J.; Szpoganicz, B.; Severino, P. C.; Terenzi, H.; Tomkowicz, Z.; Ostrovsky, S.; Haase, W.; Ozarowski, A.; Krzystek, J.; Telser, J.; Schenk, G.; Gahan, L. R. *Inorg. Chem.* **2009**, *48*, 7905−7921.
(56) Peter Comba, P.; Gahan, L. R.; Hanson, G. R.; Mereacre, V.; Noble, C. J.; Powel, A. K.; Prisecaru, I.; Schenk, G.; Zajaczkowski-Fischer, M. *Chem.—Eur. J.* **2011**, (in Press). DOI: 10.1002/chem.201100229.
(57) Jeon, J. W.; Son, S. J.; Yoo, C. E.; Hong, I. S.; Song, J. B.; Suh, J. *Org. Lett.* **2002**, *4*, 4155−4158.
(58) Hegg, E. L.; Burstyn, J. N. *J. Am. Chem. Soc.* **1995**, *117*, 7015−7016.
(59) Oliveira, M. C. B.; Mazera, D.; Scarpellini, M.; Severino, P. C.; Neves, A.; Terenzi, H. *Inorg. Chem.* **2009**, *48*, 2711−2713.
(60) Maity, B.; Roy, M.; Saha, S.; Chakravarty, A. R. *Organometallics* **2009**, *28*, 1495−1505.
(61) Roy, M.; Bhowmick, T.; Santhanagopal, R.; Ramakumar, S.; Chakravarty, A. R. *Dalton Trans.* **2009**, 4671−4682.
(62) Zhang, H.-X.; Gao, S.; Xiong, Z.-Y.; Liu, S.-P. *Mol. Biol. Rep.* **2009**, *36*, 2299−2306.
(63) Gharagozlou, M.; Boghaei, D. M. *Spectrochim. Acta, Part A: Mol. Biomol. Spectrosc.* **2008**, *71*, 1617−1622.
(64) Xu, M.; Chen, F.-J.; Huang, L.; Xi, P.-X.; Zeng, Z.-Z. *J. Lumin.* **2011**, *131*, 1557−1565.
(65) Toneatto, J.; Argüello, G. A. *J. Inorg. Biochem.* **2011**, *105*, 645−651.
(66) Smoukov, S. K.; Quaroni, L.; Wang, X.; Doan, P. E.; Hoffman, B. M.; Que, L. Jr. *J. Am. Chem. Soc.* **2002**, *124*, 2595−2603.
(67) Borovik, A. S.; Murch, B. P.; Que, L. Jr.; Papaefthymiou, V.; Münch, E. *J. Am. Chem. Soc.* **1987**, *109*, 7190−7191.
(68) Bernal, I.; Jensen, I. M.; Jensen, K. B.; McKenzie, C. J.; Toftlund, H.; Tuchagues, J.-P. *J. Chem. Soc., Dalton Trans.* **1995**, 3667−3675.
(69) Simaan, J.; Poussereau, S.; Blondin, G.; Girerd, J.-J.; Defaye, D.; Philouze, C.; Guilhem, J.; Tchertanov, L. *Inorg. Chim. Acta* **2000**, *299*, 221−230.

(70) Davydov, R. M.; Smieja, J.; Dikanov, S. A.; Zang, Y.; Que, L. Jr.; Bowman, M. K. *J. Biol. Inorg. Chem.* **1999**, *49*, 292−301.
(71) Hartman, J. R.; Rardin, R. L.; Chaudhuri, P.; Pohl, K.; Wieghardt, K.; Nuber, B.; Weiss, J.; Papaefthymiou, G. C.; Frankel, R. B.; Lippard, S. J. *J. Am. Chem. Soc.* **1987**, *109*, 7387−7396.
(72) Mashuta, M. S.; Webb, J.; McCusker, J. K.; Schmitt, E. A.; Oberhausen, K. J.; Richardson, J. F.; Buchanan, R. M.; Hendrickson, D. N. *J. Am. Chem. Soc.* **1992**, *114*, 3815−3827.
(73) Payne, S. C.; Hagen, K. S. *J. Am. Chem. Soc.* **2000**, *122*, 6399−6410.
(74) Berthold, D. A.; Voevodskaya, N.; Stenmark, P.; Graslund, A.; Nordlund, P. *J. Biol. Chem.* **2002**, *277*, 43608−43614.
(75) Atta, M.; Andersson, K. K.; Ingemarson, R.; Thelander, L.; Graslund, A. *J. Am. Chem. Soc.* **1994**, *116*, 6429−6430.
(76) Davydov, R. M.; Davydov, A.; Ingemarson, R.; Thelander, L.; Ehrenberg, A.; Graslund, A. *Biochemistry* **1997**, *36*, 9093−9100.
(77) Ravi, N.; Prickril, B. C.; Kurtz, D. M.; Huynh, B. H. *Biochemistry* **1993**, *32*, 8487−8491.
(78) Tatur, J.; Hagen, W. R. *FEBS Lett.* **2005**, *579*, 4729−4732.
(79) Xing, G.; Hoffart, L. M.; Diao, Y.; Prabhu, K. S.; Arner, R. J.; Reddy, C. C.; Krebs, C.; Bollinger, J. M. *Biochemistry* **2006**, *45*, 5393−5401.
(80) Yu, L.; Golbeck, J.; Yao, J.; Rusnak, F. *Biochemistry* **1997**, *36*, 10727−10734.
(81) Yu, L.; Haddy, A.; Rusnak, F. *J. Am. Chem. Soc.* **1995**, *117*, 10147−10148.
(82) Mitic, N.; Schenk, G.; Hanson, G. R. In *Biological magnetic resonance: high resolution EPR: applications to metalloenzymes and metals in medicine*; Hanson, G. R., Berliner, L. J., Eds.; Springer: New York, 2008; Vol. *28*.
(83) Day, E.; David, S.; Peterson, J.; Dunham, W.; Bonvoisin, J.; Sands, R.; Que, L. Jr. *J. Biol. Chem.* **1988**, *263*, 15561−15567.
(84) Debrunner, P. G.; Hendrich, M. P.; de Jersey, J.; Keough, D. T.; Sage, J. T.; Zerner, B. *Biochim. Biophys. Acta* **1983**, *745*, 103−106.
(85) Antanaitis, B. C.; Aisen, P. *J. Biol. Chem.* **1982**, *257*, 5330−5332.
(86) Crowder, M. W.; Vincent, J. B.; Averill, B. A. *Biochemistry* **1992**, *31*, 9603−9608.
(87) Merkx, M.; Pinkse, M. W. H.; Averill, B. A. *Biochemistry* **1999**, *38*, 9914−9925.
(88) Antanaitis, B. C.; Aisen, P. *J. Biol. Chem.* **1985**, *260*, 751−756.
(89) Aquino, M. A. S.; Lim, J.-S.; Sykes, A. G. *J. Chem. Soc., Dalton Trans.* **1994**, 429−436.
(90) Aquino, M. A. S.; Sykes, A. G. *J. Chem. Soc., Dalton Trans.* **1994**, 683−687.
(91) Grillo, V. A.; Hanson, G. R.; Wang, D.; Hambley, T. W.; Gahan, L. R.; Murray, K. S.; Moubaraki, B.; Hawkins, C. J. *Inorg. Chem.* **1996**, *35*, 3568−3576.
(92) Holgate, S. J. W.; Bondarenko, G.; Collison, D.; Mabbs, F. E. *Inorg. Chem.* **1999**, *38*, 2380−2385.
(93) Ozarowski, A.; McGarvey, B. R.; Drake, J. E. *Inorg. Chem.* **1995**, *34*, 5558−5566.
(94) Mitić, N.; Noble, C. J.; Gahan, L. R.; Hanson, G. R.; Schenk, G. *J. Am. Chem. Soc.* **2009**, *131*, 8173.
(95) Murray, K. S. *Coord. Chem. Rev.* **1974**, *12*, 1−35.
(96) Accorsi, S.; Barra, A.-L.; Caneschi, A.; Chastanet, G.; Cornia, A.; Fabretti, A. C.; Gatteschi, D.; Mortalo, C.; Olivieri, E.; Parenti, F.; Rosa, P.; Sessoli, R.; Sorace, L.; Wernsdorfer, W.; Zobbi, L. *J. Am. Chem. Soc.* **2006**, *128*, 4742−4755.
(97) Datta, S.; Waldmann, O.; Kent, A. D.; Milway, V. A.; Thompson, L. K.; Hill, S. *Phys. Rev. B* **2007**, *76*, 052407.
(98) Liviotti, E.; Carretta, S.; Amoretti, G. *J. Chem. Phys.* **2002**, *117*, 3361−3368.
(99) Gehring, S.; Fleischhauer, P.; Behlendorf, M.; Huber, M.; Lorosch, J.; Haase, W.; Dietrich, M.; Witzel, H.; Locke, R.; Krebs, B. *Inorg. Chim. Acta* **1996**, *252*, 13−17.
(100) Horn, A.; Neves, A.; Vencato, I.; Drago, V.; Zucco, C.; Werner, R.; Haase, W. *J. Braz. Chem. Soc.* **2000**, *11*, 7−10.
(101) Neves, A.; Rossi, L. M.; Vencato, I.; Haase, W.; Werner, R. *J. Chem. Soc., Dalton Trans.* **2000**, 707−712.
(102) Bernard, E.; Chardon-Noblat, S.; Deronzier, A.; Latour, J.-M. *Inorg. Chem.* **1999**, *38*, 190−193.
(103) Lanznaster, M.; Neves, A.; Bortoluzzi, A. J.; Aires, V. V. E.; Szpoganicz, B.; Terenzi, H.; Severino, P. C.; Fuller, J. M.; Drew, S. C.; Gahan, L. R.; Hanson, G. R.; Riley, M. J.; Schenk, G. *J. Biol. Inorg. Chem.* **2005**, *10*, 319−332.
(104) Schenk, G.; Peralta, R. A.; Batista, S. C.; Bortoluzzi, A. J.; Szpoganicz, B.; Dick, A. K.; Herrald, P.; Hanson, G. R.; Szilagyi, R. K.; Riley, M. J.; Gahan, L. R.; Neves, A. *J. Biol. Inorg. Chem.* **2008**, *13*, 139−155.
(105) Mitić, N.; Valizadeh, M.; Leung, E. W. W.; de Jersey, J.; Hamilton, S.; Hume, D. A.; Cassady, A. I.; Schenk, G. *Arch. Biochem. Biophys.* **2005**, *439*, 154−164.
(106) Valizadeh, M.; Schenk, G.; Nash, K.; Oddie, G. W.; Guddat, L. W.; Hume, D. A.; de Jersey, J.; Burke, J.; Terrence, R.; Hamilton, S. *Arch. Biochem. Biophys.* **2004**, *424*, 154−162.
(107) Neves, A.; Lanznaster, M.; Bortoluzzi, A. J.; Peralta, R. A.; Casellato, A.; Castellano, E. E.; Herrald, P.; Riley, M. J.; Schenk, G. *J. Am. Chem. Soc.* **2007**, *129*, 7486−7487.
(108) Karsten, P.; Neves, A.; Bortoluzzi, A. J.; Lanznaster, M.; Drago, V. *Inorg. Chem.* **2002**, *41*, 4624−4626.
(109) Barrios, A. M.; Lippard, S. J. *J. Am. Chem. Soc.* **1999**, *121*, 11751−11757.
(110) Burgess, J. *Metal Ions in Solution*; Ellis Horwood: Chichester, U.K., 1978.
(111) Wu, F.-J.; Kurtz, D. M.; Hagen, K. S.; Nyman, P. D.; Debrunner, P. G.; Vankai, V. A. *Inorg. Chem.* **1990**, *29*, 5174−5183.
(112) Hartman, J. R.; Rardin, R. L.; Chaudhuri, P.; Pohl, K.; Wieghardt, K.; Nuber, B.; Weiss, J.; Papaefthymiou, G. C.; Frankel, R. B.; Lippard, S. J. *J. Am. Chem. Soc.* **1987**, *109*, 7387−7396.
(113) Parrilha, G. L.; Fernandes, C.; Bortoluzzi, A. J.; Szpoganicz, B.; Silva, M.; Pich, C. T.; Terenzi, H.; Horn, A. *Inorg. Chem. Commun.* **2008**, *11*, 643−647.
(114) Lanznaster, M.; Neves, A.; Bortoluzzi, A. J.; Szpoganicz, B.; Schwingel, E. *Inorg. Chem.* **2002**, *41*, 5641−5643.
(115) Smith, S. J.; Casellato, A.; Hadler, K. S.; Mitic, N.; Riley, M. J.; Bortoluzzi, A. J.; Szpoganicz, B.; Schenk, G.; Neves, A.; Gahan, L. R. *J. Biol. Inorg. Chem.* **2007**, *12*, 1207−1220.
(116) Schenk, G.; Elliot, T. W.; Leung, E.; Carrington, L. E.; Mitic, N.; Gahan, L. R.; Guddat, L. W. *BMC Struct. Biol.* **2008**, *8*, 6.
(117) Twitchett, M. B.; Sykes, A. G. *Eur. J. Inorg. Chem.* **1999**, 2105−2115.
(118) Klabunde, T.; Sträter, N.; Frohlich, R.; Witzel, H.; Krebs, B. *J. Mol. Biol.* **1996**, *259*, 737−748.
(119) Cox, R. S.; Schenk, G.; Mitić, N.; Gahan, L.; Hengge, A. C. *J. Am. Chem. Soc.* **2007**, *129*, 9550−9551.
(120) Mitić, N.; Hadler, K. S.; Gahan, L. R.; Hengge, A. C.; Schenk, G. *J. Am. Chem. Soc.* **2010**, *132*, 7049−7054.